ChemComm

FEATURE ARTICLE

View Article Online
View Journal | View Issue

Cite this: *Chem. Commun.*, 2020, **56**, 10419

Crystal engineering of porous coordination networks to enable separation of C2 hydrocarbons

Soumya Mukherjee, *[ab] Debobroto Sensharma, [a] Kai-Jie Chen *[c] and Michael J. Zaworotko *[a]

Received 5th July 2020,
Accepted 31st July 2020

DOI: 10.1039/d0cc04645k

rsc.li/chemcomm

Crystal engineering, the field of chemistry that studies the design, properties, and applications of crystals, is exemplified by the emergence over the past thirty years of porous coordination networks (PCNs), including metal–organic frameworks (MOFs) and hybrid coordination networks (HCNs). PCNs have now come of age thanks to their amenability to design from first principles and how this in turn can result in new materials with task-specific features. Herein, we focus upon how control over the pore chemistry and pore size of PCNs has been leveraged to create a new generation of physisorbents for efficient purification of light hydrocarbons (LHs). The impetus for this research comes from the need to address LH purification processes based upon cryogenic separation, distillation, chemisorption or solvent extraction, each of which is energy intensive. Adsorptive separation by physisorbents (in general) and PCNs (in particular) can offer two advantages over these existing approaches: improved energy efficiency; lower plant size/cost. Unfortunately, most existing physisorbents suffer from low uptake and/or poor sorbate selectivity and are therefore unsuitable for trace separations of LHs including the high volume C2 LHs (C_2H_x, x = 2, 4, 6). This situation is rapidly changing thanks to PCN sorbents that have set new performance benchmarks for several C2 separations. Herein, we review and analyse PCN sorbents with respect to the supramolecular chemistry of sorbent–sorbate binding and detail the crystal engineering approaches that have enabled the exquisite control over pore size and pore chemistry that affords highly selective binding sites. Whereas the structure–function relationships that have emerged offer important design principles, several development roadblocks remain to be overcome.

1. Introduction

The chemical industry has a turnover of $5.7 trillion per annum which represents *ca.* 7% of global GDP.[1] Its energy footprint is even higher, with separation/purification of chemical commodities accounting for *ca.* 40% of industrial energy consumption. This underscores the societal need for greater energy efficiency and sustainability in the production of chemicals[2] given that this energy footprint represents *ca.* 15% of global energy consumption.[3] Further, there has been a forecast that suggests a threefold increase in demand for chemical commodities by 2050.[2] The main reason for the energy footprint of commodity purification is reliance upon energy-intensive separation methods such as cryogenic separation, azeotropic and/or fractional distillation, chemisorption and solvent extraction.[4]

Key to reducing the energy footprint of separations in today's 'Age of Gas'[2] are new technologies for gas and vapour purification. In this context, light hydrocarbon (LH) production is ever-increasing[5] and chemists, material scientists and process engineers have been addressing the development of potentially disruptive energy-efficient LH separation processes that could be enabled by porous physisorbents.[6] Herein, we address the rapid evolution of a new generation of physisorbents that have made significant progress with respect to addressing C2 LH purification, ethylene (C_2H_4), acetylene (C_2H_2) and ethane (C_2H_6).

Why C2 separations matter

Millions of tonnes of C2 LHs are produced every year from coal, petroleum, and natural gas using a network of interrelated chemical processes and purification steps (Fig. 1). C_2H_4 is one of the highest volume products of the chemical industry and is

[a] *Bernal Institute, Department of Chemical Sciences, University of Limerick, Limerick V94 T9PX, Republic of Ireland. E-mail: xtal@ul.ie*
[b] *Catalysis Research Center, Ernst-Otto-Fischer Straße 1 and Department of Chemistry, Technical University of Munich, Lichtenbergstraße 4, 85748 Garching bei München, Germany. E-mail: soumya.mukherjee@tum.de*
[c] *Key Laboratory of Special Functional and Smart Polymer Materials of Ministry of Industry and Information Technology, School of Chemistry and Chemical Engineering, Northwestern Polytechnical University, Xi'an, Shaanxi, 710072, China. E-mail: ckjiscon@nwpu.edu.cn*

the basic building block for a variety of polymers, solvents, detergents and coatings. The recent shale gas boom has reduced C_2H_4 costs by approximately half in Europe and North America in the past ten years, and this has consolidated its position as the "*backbone of the global chemical industry*."[2,7,8] The quantity of C_2H_4 produced annually was estimated to be *ca.* 143 Mt per year with a market value of US$254.6 billion in 2016. This is projected to reach US$475.8 billion in 2023 with an approximate growth rate of 5% per year.[9,10] Although there is a wide variety of industrial uses for C_2H_4, over 80% of C_2H_4 production in the US, Europe and Japan is for the production of polyethylene, ethylene oxide and ethylene chlorides.[11,12] Impurities in such processes can have substantial negative impacts on productivity.[13] For example, if >5 ppm of C_2H_2 is present in C_2H_4 during polymerisation, the catalyst can become poisoned and its recovery is limited. Typically, polymer-grade specifications require C_2H_4 of $>99.9\%$ purity, with <2 ppm C_2H_2 and <200 ppm C_2H_6 and methane.[12]

C_2H_4 is produced primarily by the steam cracking of C_2H_6 and light naphtha, with a small additional contribution from the hydrogenation of C_2H_2. During production from C_2H_6, C_2H_4 is typically the major product and C_2H_4/C_2H_6 separation is needed to remove C_2H_6 from incomplete conversion.

Soumya Mukherjee

After receiving his undergraduate and postgraduate degrees from the University of Calcutta (India), Soumya Mukherjee earned his PhD in Inorganic Chemistry under the tutelage of Prof. Sujit K. Ghosh at the Indian Institute of Science Education and Research (IISER) Pune (India) in 2017. Soumya worked as a Science Foundation of Ireland (SFI) funded postdoctoral researcher with Prof. Mike Zaworotko at the Bernal Institute, University of Limerick (Ireland) for three years until 2019. A recipient of the Alexander von Humboldt (AvH) research fellowship and an awarded member of the Royal Society of Chemistry (MRSC), Soumya is keen to develop crystal engineered porous materials that can address global challenges of the current times, particularly materials for energy and environmental sustainability.

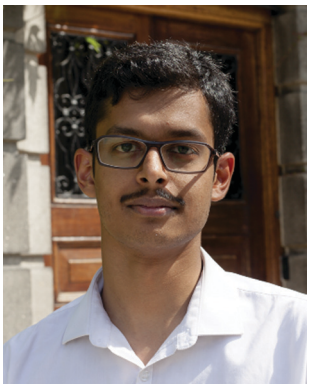

Debobroto Sensharma

Debobroto Sensharma received his undergraduate degree from St. Stephen's College, University of Delhi in 2014 and won the Mohan Katyal Memorial chemistry prize. Following a brief stint working on organoselenium compounds at the lab of Prof. G. Mugesh at the Indian Institute of Science, he then began his PhD on flexible and topologically unusual coordination polymers under Prof. Wolfgang Schmitt at Trinity College Dublin, with a Trinity Research Studentship. After completing his PhD in 2019, he joined the group of Prof. Michael J. Zaworotko at the Bernal Institute, where his postdoctoral research is on the development of next-generation metal–organic materials.

Kai-Jie Chen

Kai-Jie Chen finished his undergraduate study in 2008 at Zhengzhou University, and earned his PhD under the supervision of Prof. Xiao-Ming Chen from Sun Yat-Sen University in 2013. Then he conducted the postdoctoral research in Prof. Michael J. Zaworotko's group at University of Limerick from 2014 to 2018. After that, he joined Northwestern Polytechnical University in 2018 as a full professor. His current research interest is focused on crystal engineering of porous coordination polymers (especially for design of task-specific ultramicropores through exquisite control on pore chemistry and pore size) and related gas separation application.

Michael J. Zaworotko

Dr Mike Zaworotko was born in Wales in 1956 and received his BSc and PhD degrees from Imperial College (1977) and the University of Alabama (1982), respectively. He served as a faculty member at Saint Mary's University, Nova Scotia, Canada, from 1985–1998, at University of Winnipeg, Canada from 1998–1999 and at the University of South Florida, USA, from 1999–2013. In 2013 he joined the University of Limerick, Ireland, where he currently serves as Bernal Chair of Crystal Engineering and Co-Director of the Synthesis and Solid-State Pharmaceutical Centre. Current research interest include the design of metal–organic materials, especially microporous and ultramicroporous sorbents, and multi-component pharmaceutical materials such as cocrystals, hydrates and ionic cocrystals.

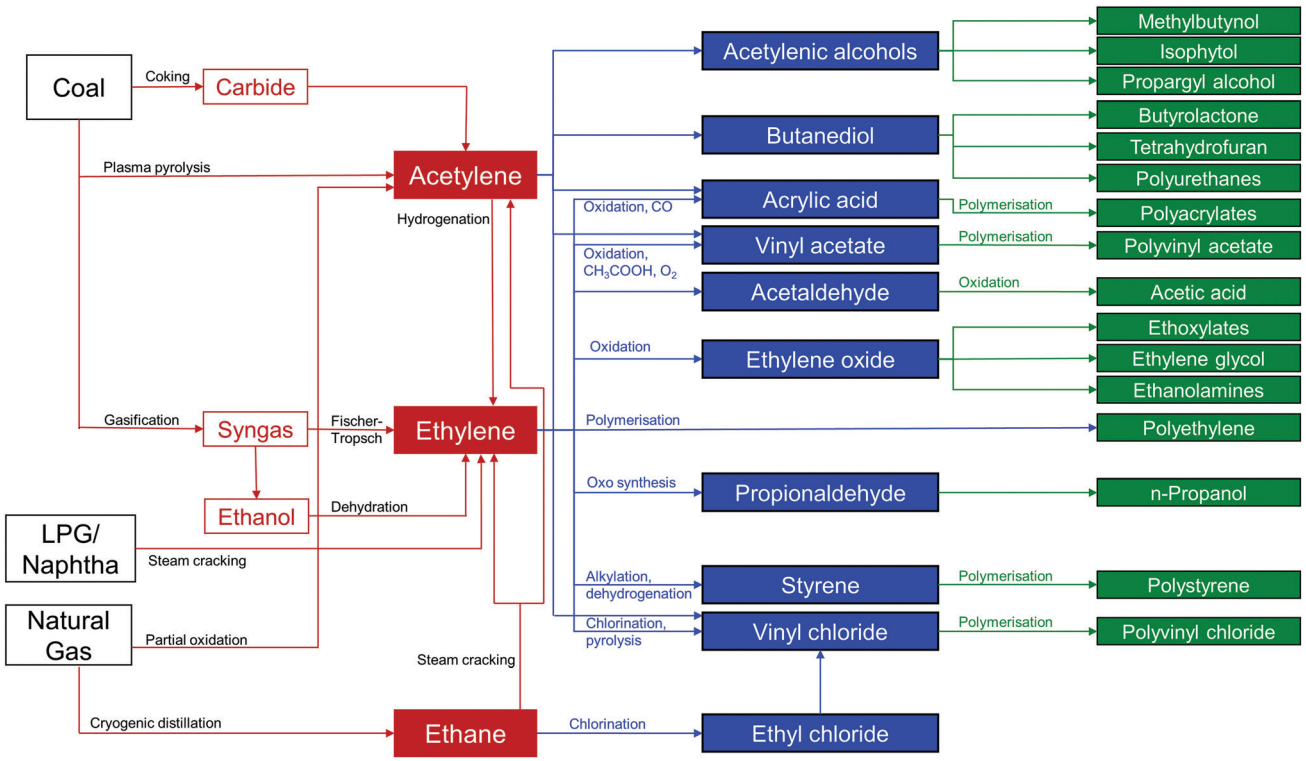

Fig. 1 A schematic of industrial routes for the production of C2 hydrocarbons and derived products.

Production by cracking of naphtha, affords C_2H_4 and propylene as the major products, but other C_2–C_6 olefins are present in significant quantities and a complex separation pathway is utilised.[12] These processes require separation of C2 LHs from each other, a challenging proposition because of their similar boiling points, molecular sizes and properties (Fig. 2).[14–16] Due in large part to these separation processes, the production of light olefins by steam cracking is the most energy-intensive process in the chemical industry, accounting for *ca.* 20% of its energy footprint and around 30% of its CO_2 emission.[7,17]

C_2H_2 is also a major chemical building block. Production volumes have decreased from 10 Mt per year in 1960 to hundreds of kt per year at present, overtaken by cheaper, safer C_2H_4 as the C_2 feedstock of choice after the shift from coal to a petroleum-based industrial economy.[2,18–20] Nonetheless, C_2H_2 production is increasing again and the processes used for C_2H_2 all involve high temperatures; C_2H_2 is the most thermodynamically stable of the C2 LHs at temperatures above 1400 K.[21,22] Partial oxidation of natural gas is an increasingly important route to C_2H_2 due to relatively low natural gas prices. C_2H_2 recovered by separation as a by-product of C_2H_4 production is also often commercially viable.[18] C_2H_2 used as fuel in oxy-acetylene torches does not typically need to be highly pure (*ca.* 98%),[22] however, for use as a chemical feedstock, high purity C_2H_2 is needed. For example, specifications for 'Type A' C_2H_2 in India require >99 volume% and <0.15% H_2S, <0.1% NH_3, <0.06% phosphine, <0.006% arsine when produced from the carbide process.[23]

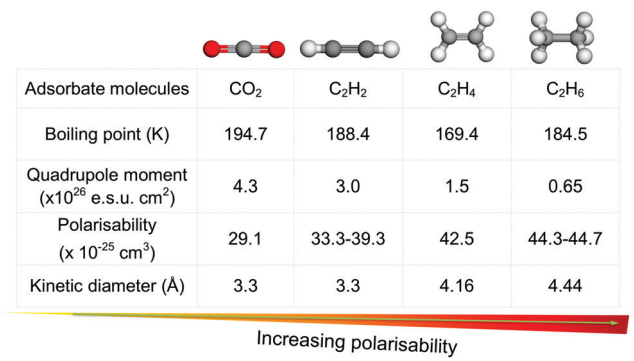

Adsorbate molecules	CO_2	C_2H_2	C_2H_4	C_2H_6
Boiling point (K)	194.7	188.4	169.4	184.5
Quadrupole moment ($x10^{26}$ e.s.u. cm^2)	4.3	3.0	1.5	0.65
Polarisability ($x\ 10^{-25}$ cm^3)	29.1	33.3-39.3	42.5	44.3-44.7
Kinetic diameter (Å)	3.3	3.3	4.16	4.44

Fig. 2 Comparison of key physicochemical properties of CO_2 and C2 LHs reveals the similarities in properties for multiple industrially relevant gas pairs.

C_2H_6 is the second most abundant component of natural gas (0.7–6.8%).[24] Approximately 40% of C_2H_6 is recovered for chemical use, mainly as a feedstock in steam cracking. Purified C_2H_6 is used in small amounts in the synthesis of chloroethane.[25] Purification of C2 LHs is therefore central to the chemical industry as a whole and represents a major portion of its energy usage and, in turn, global energy production. This means that, because of the production scale of C2 LHs and their derivatives, even minor improvements to purification processes could result in major economic and/or energy savings.

Why porous coordination networks, PCNs, promise to deliver on the challenge of C2 LH separations

That composition and structure profoundly impact the properties of crystalline solids has provided impetus for exponential growth in the field of crystal engineering over the past 30 years.

Crystal engineering, the field of chemistry that studies the design, properties and applications of crystals, has evolved from focus upon structure (form) towards control over bulk properties (function).[26] Crystal engineering now offers a paradigm shift from the more random, high-throughput methods that have traditionally been utilised in materials discovery and development. This situation is exemplified by porous physisorbents such as PCNs, a term coined by Ma and Zhou in the early 2000s.[27] In essence, crystal engineering of PCNs has come of age thanks to their inherent modularity and two decades of ever-increasing activity from materials chemists who are now aiming to design the right material for the right application.[28]

A subset of PCNs, metal–organic materials, MOMs,[29] are particularly amenable to crystal engineering design principles that allow for ''bottom-up'' design approaches of a new generation of crystalline porous physisorbents suitable for application in commodity gas separations.[4,15] The composition of PCNs makes them inherently amenable to design from first principles; they are typically comprised of metal cations or metal ''node'' clusters linked into 2D or 3D potentially porous networks by organic and/or inorganic ''linker'' ligands. This ''node-and-linker'' concept of designing specific structural motifs was introduced by Robson and Hoskins in 1989[30] and has subsequently afforded tens of thousands of CNs that can potentially exhibit permanent porosity.[31] The potential utility of permanent porosity motivated Kitagawa and Yaghi to coin the terms PCPs, porous coordination polymers,[32] and MOFs, metal–organic frameworks, respectively.[33]

1999 saw the seminal discoveries of the first two examples of extra-large surface-area PCNs: HKUST-1[34] [Cu_3(1,3,5-benzenetricarboxylate)$_2$]$_n$, *ca.* 1900 $m^2\ g^{-1}$; MOF-5[35] [Zn_4O(1,4-benzenedicarboxylate)$_3$]$_n$, *ca.* 3800 $m^2\ g^{-1}$. The quest for ultra-high surface area MOFs continues, with recent benchmarks set by DUT-60 (7839 $m^2\ g^{-1}$) and NU-110 (7140 $m^2\ g^{-1}$).[36,37] Ironically, it is PCNs featuring much smaller pores *i.e.* ultramicropores ($<$0.7 nm), that are the focus herein. This is because ultramicropores tend to outperform other classes of physisorbents with respect to separation performance driven by selective binding of gases and optimal thermodynamics/kinetics. Ultramicropores function well in this context as they combine tight sorbent–sorbate binding with fine-tuned pore chemistry. Such selective binding is key to enabling separation of hard-to-separate gas molecules with similar size, shape and physical properties, as exemplified by hybrid ultramicroporous materials (HUMs).[28] HUMs directly address a major weakness of most physisorbents, which bind sorbates too weakly to separate trace gas impurities from mixtures under ambient conditions. This is because HUMs offer energetic ''sweet spots'', binding sites that are not too strong and not too weak, for a number of gas separations involving CO_2,[38–40] C_2H_2,[41,42] and H_2O.[43,44] It has become apparent that ultramicroporous PCNs have emerged as the top-performing sorbents for gas separation and purification,[45] as we detail herein with respect to C2 LHs. Notably, this means that interpenetration in HUMs, a phenomenon once considered detrimental to porosity,[46] is key to controlling pore size and enabling tight C2 LH binding sites that result in exceptional sorption performance.[41,42,47]

2. The industrial state-of-the-art in C2 LH separations

Steam cracking accounts for a large share of the energy used by the chemical industry because of the high temperatures required for the pyrolysis of hydrocarbons. Nevertheless, 35–50% of the energy used in C_2H_4 production comes from the fractionation, compression and separation processes required to produce pure C_2H_4.[7] In a typical process, C_2H_4 and other steam cracking products are separated by cryogenic distillation at conditions as extreme as 183–258 K and 7–28 bar compounded with $>$100 tray numbers and reflux ratios of 2.5–4 for C_2H_4/C_2H_6 separation to meet polymer-grade specifications.[10]

C_2H_2 is also used as a feedstock but its explosive nature makes liquefaction hazardous and compression above 1.4 bar is avoided, discouraging cryogenic purification. Selective gas–liquid absorption processes are commonly used, employing solvents such as *N*-methyl pyrrolidone, *N*,*N*-dimethyl formamide, methanol, ammonia and acetone. A pre-scrubbing process is used to remove higher alkynes which tend to polymerise. Purified C_2H_2 is recovered by depressurising the solvent and elevating temperature. This process can yield C_2H_2 of $>$98.4% purity. Further treatment with aqueous H_2SO_4 and NaOH allows for recovery of 99.7% pure C_2H_2.[18]

Although gas–liquid absorption has some advantages over cryogenic distillation, it nonetheless operates at temperatures and pressures significantly above ambient, poses risks in terms of hazardous solvents and pressurised C_2H_2, and has a substantial energy cost. Further, the poor selectivity of solvents like *N*-methyl pyrrolidone for C_2H_2 over CO_2 (present in high abundance in raw C_2H_2 streams, especially from partial oxidation) necessitates additional scrubbing steps using ammonia and NaOH.[18,48,49]

Gas–liquid absorption methods are also used for the recovery of C_2H_6 from natural gas streams. The heavier impurities, such as propane and butane, are absorbed into a ''lean'' absorption oil, while the light C_2H_6 fraction remains in the natural gas stream. Although this approach is less energy intensive than cryogenic distillation, it has much lower efficiency, and cryogenic techniques are generally preferred in industry.[50] The cryogenic technique involves cooling natural gas to 188 K using an expansion turbine coupled with a fractionating column and liquefying the C_2 and heavier fractions while methane, CH_4, remains in the natural gas stream.[25]

In summary, the industrial state-of-the-art for purification of C_2H_2, C_2H_4 and C_2H_6 involves energy-intensive processes that are conducted at non-ambient conditions and industrial purification of chemical products accounts for *ca.* 15% of global energy production. It is therefore unsurprising that replacing such processes with sorbent-based separations that yield high purity C2 LHs and operate at near-ambient conditions was highlighted by Scholl and Lively as one of the seven ''separations to change the world.''[3,51] The processes outlined above purify C2 LHs from a variety of impurities including CH_4, heavier hydrocarbons, and sulphur compounds, as well as purifying C_2H_4 and C_2H_2 from by-products. Herein, we address

how and why PCNs have recently become the benchmark physisorbents for several C2 binary separations: CO_2/C_2H_2,[47] C_2H_2/CO_2,[52–54] C_2H_2/C_2H_4,[52,55,56] C_2H_4/C_2H_6,[57–59] and C_2H_6/C_2H_4.[60,61]

3. Chronology of key discoveries in the utility of PCNs as C2 sorbents

Interest in the utility of PCNs for C2 separations is a relatively recent phenomenon. As revealed by Fig. 3, the number of reported studies has grown exponentially over the past decade, especially since 2015. Prior to 2005, before PCNs were widely studied for gas separations, research tended to focus upon C_2H_4/C_2H_6, then considered the most important binary separation in industrial processes.[3] In 2005, a 2D MOF, CPL-1, was reported by the Kitagawa group to possess excellent C_2H_2/CO_2 selectivity and therefore offer potential for use in separations.[62] To separate this pair of gas molecules, which exhibit identical kinetic diameters (Fig. 2), precise pore size/chemistry is needed, as subsequently demonstrated by several research groups (Fig. 4). For example, "Yin–Yang" separation of C_2H_2 and CO_2 in two closely related HUMs (**TIFSIX-2-Cu-i** and **SIFSIX-3-Ni**) was realised in 2016 by the Zaworotko group thanks to the different pore structure of these two chemically related HUMs.[47] In 2019, reverse C_2H_2/CO_2 separation in two isostructural HUMs (**SIFSIX-3-Ni** and ZJUT-2) was achieved by B. Chen and Hu's groups.[63] Most recently, two ultramicroporous PCNs (TCuCl and ZJU-74) were published by the Zaworotko and Qian groups, respectively.[64] These materials were found to exhibit benchmark C_2H_2 capture performance from CO_2 in terms of separation selectivity and uptake capacity, respectively.

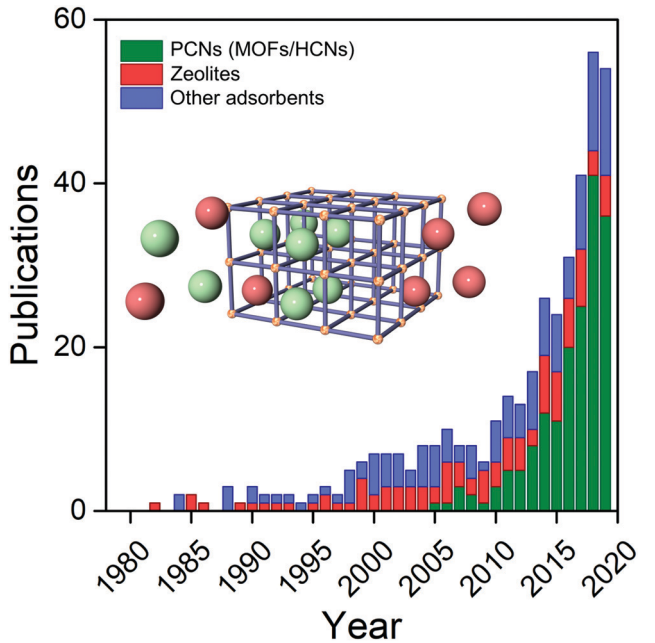

Fig. 3 Scopus search results for publications on adsorptive separation of C2 hydrocarbons from 1979 to 2019 colour coded by type of material studied (inset: schematic illustration of C2 separation from binary LH mixtures).

For C_2H_2/C_2H_4 separation, high adsorption selectivity by a flexible PCN was reported in 2011 by B. Chen's group.[65] In 2016, **SIFSIX-1-Cu** and **SIFSIX-2-Cu-i** were reported by the Xing, B. Chen and Zaworotko groups to deliver record-high C_2H_2 adsorption selectivity over C_2H_4.[41] Another variant in this platform, **SIFSIX-14-Cu-i** (also known as UTSA-200a) was reported in 2017 to exhibit a sieving effect for C_2H_2 over C_2H_4.[42] Regarding C_2H_4 *vs.* C_2H_6, C_2H_4 selectivity in Fe-MOF-74 and NOTT-300 was reported by the Long and Schröder groups, respectively.[66,67] These PCNs offer high C_2H_4 working capacities and moderate selectivity values. In 2018, the first, and thus far only, example of a C_2H_4 sieving PCN over C_2H_6, UTSA-280, was reported by B. Chen's group to exhibit ultra-high adsorption selectivity of $>10^4$.[57] UTSA-280 also offers low production cost even when upscaled.

C_2H_6 selective adsorbents feature the advantage of incurring a minimal energy footprint during C_2H_4 production because a single-step adsorption process would purify C_2H_4 and replace the energy penalty for the regeneration process based upon C_2H_4 selective physisorbents. In this context, an azolate ultramicroporous material (AUM), MAF-49, first reported by Zhang and X.-M. Chen's group in 2015, was reported to exhibit record-high C_2H_6 adsorption energy and benchmark low-pressure uptake.[68]

In 2018, Fe-MOF-74 was post-synthetically modified with Fe–peroxo sites by B. Chen and Li's groups to afford $Fe_2(O_2)$-(dobdc), which delivered inverse C_2H_6/C_2H_4 separation and continues to be the selectivity benchmark.[60] To enable one-step C_2H_4 production, multiple impurities were removed in 2018 by an ionic PCN (TJT-100) *via* selective adsorption of C_2H_6 and C_2H_2 over C_2H_4. Zhou and Lu's findings on TJT-100 revealed co-adsorption of C_2H_6 and C_2H_2 to yield C_2H_4.[70]

The discovery of sorbate-specific physisorbents that cover a range of sorbates and are selective enough for trace impurity removal suggests that it is now time to change focus from binary gas mixtures to multi-component gas mixtures. In principle, a single sorbent could be suitable for one-step separation of multiple minor impurities but would require high selectivity for several gases over the bulk component that is being purified. Alternatively, a series of custom sorbents, each one highly selective for one of the impurities in a gas mixture, would be expected to remove minor impurities in sequence. Such an approach, termed "synergistic sorbent separation technology" (SSST), was reported in 2019 through a collaboration between the groups of K. J. Chen and Zaworotko. Three ultramicroporous physisorbents (**Zn-atz-ipa** for C_2H_6 removal, **SIFSIX-3-Ni** for trace CO_2 removal and **TIFSIX-2-Cu-i** for trace C_2H_2 removal) were packed in tandem in a single dynamic column breakthrough (DCB) setup and achieved one-step C_2H_4 production from a four-component gas mixture of $C_2H_2/C_2H_4/C_2H_6/CO_2$. This report represents the prototypal example of SSST.[71]

Whereas Fig. 4 highlights the chronology of C2 separation-related discoveries, it is far from being an exhaustive account. The C2 separation literature continues to expand and is presented in more detail in Tables 1, 2, 3 and 4, which focus upon C_2H_2/C_2H_4, C_2H_4/C_2H_6, C_2H_6/C_2H_4, C_2H_2/CO_2 and CO_2/C_2H_2, respectively.

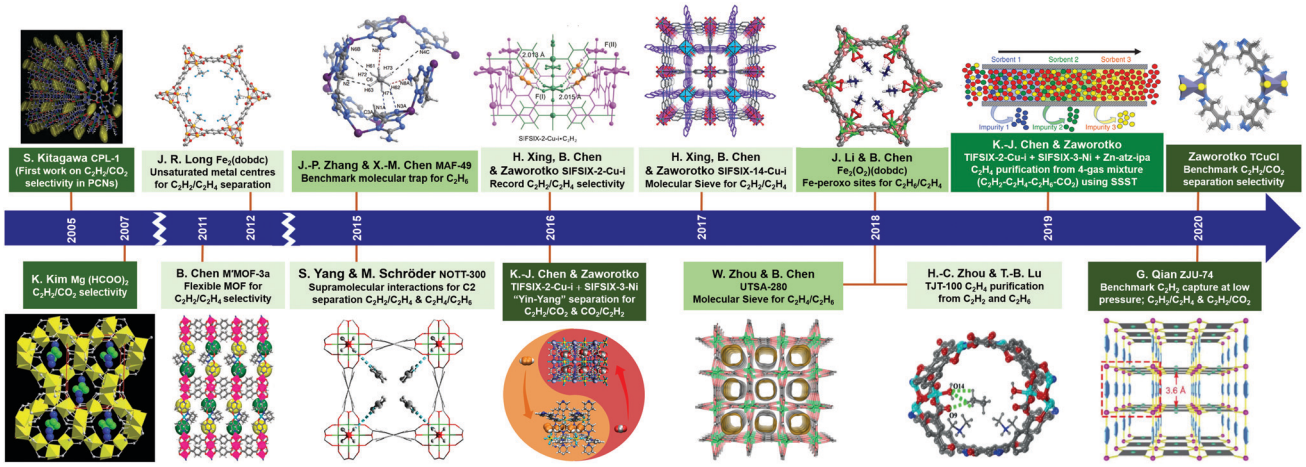

Fig. 4 Chronology of the key developments in the design and separation/purification properties of PCNs for C2 LHs. (Reprinted with permissions from ref. 62, 69, 65, 66, 68, 67, 41, 47, 42, 57, 60, 70, 71, 53 and 64; copyright 2005, Springer Nature; copyright 2007, Wiley-VCH Verlag GmbH & Co. KGaA, Weinheim; copyright 2011, Springer Nature; copyright 2012, American Association for the Advancement of Science; copyright 2015, Springer Nature; copyright 2014, Springer Nature; copyright 2016, American Association for the Advancement of Science; copyright 2016, Elsevier Inc.; copyright 2017, Wiley-VCH Verlag GmbH & Co. KGaA, Weinheim; copyright 2018, Springer Nature; copyright 2018, American Association for the Advancement of Science; copyright 2018, Wiley-VCH Verlag GmbH & Co. KGaA, Weinheim; copyright 2019, American Association for the Advancement of Science; copyright 2020, Wiley-VCH Verlag GmbH & Co. KGaA, Weinheim; copyright 2020, Wiley-VCH Verlag GmbH & Co. KGaA, Weinheim.)

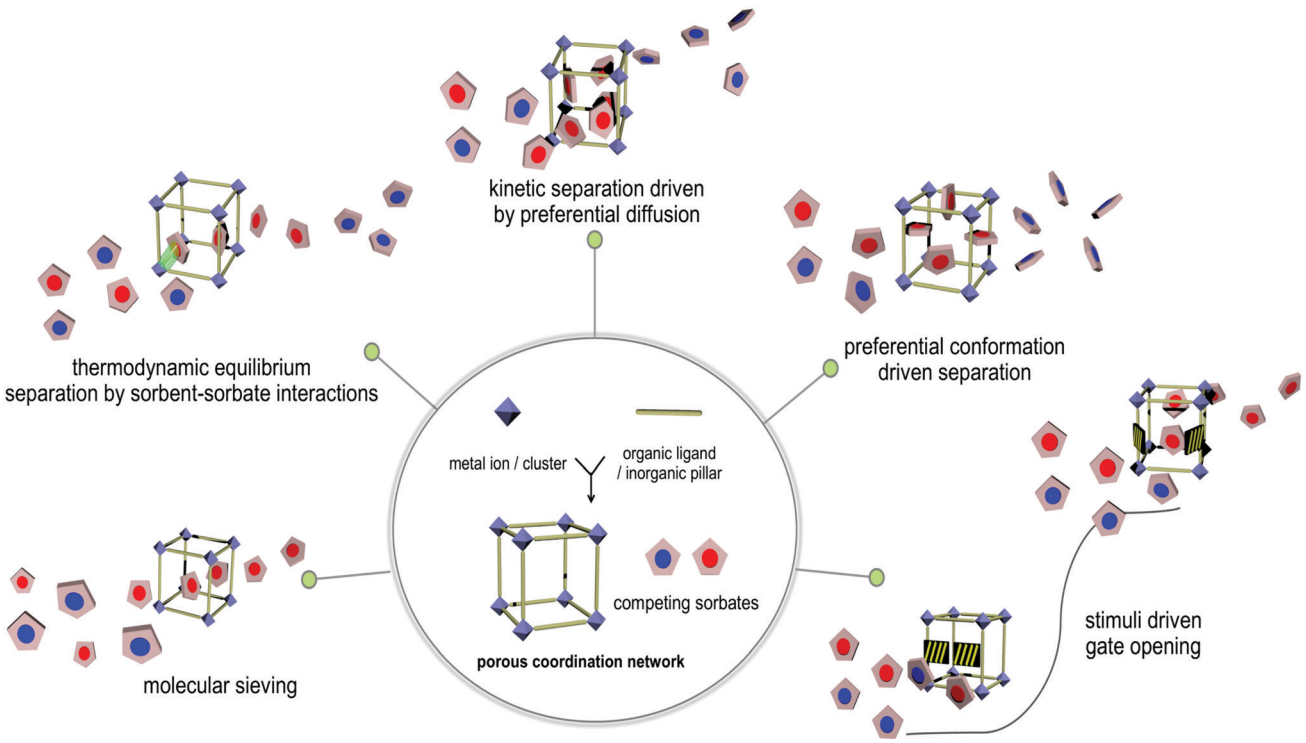

Fig. 5 There are multiple mechanisms for the adsorptive separation of C2 LHs by PCNs as illustrated clockwise from bottom left: molecular sieving by size/shape exclusion; thermodynamic equilibrium separation; differential diffusivity driven kinetic separation; conformational preference guided separation; stimuli driven network switching based upon separation concomitant with gate opening.

4. Separation of C2 gas mixtures by PCN sorbents

Whereas Section 3 details a chronology of the development of PCNs and highlights some key discoveries in the context of physisorbents with highly selective C2 binding sites, Section 4 presents an in-depth survey of the key structural and property parameters in the full range of PCNs that have been studied for C2 separations. PCN physisorbents and other classes of C2 sorbents are organised in tabular form according to parameters

Table 1 Summary of the adsorption uptakes, selectivities (S_{AE}) and adsorption enthalpies (Q_{st}) for C_2H_2 and C_2H_4 in C_2H_2 selective sorbents (arranged from top to bottom aligned with a decreasing trend of selectivities)

Adsorbent, network dimensionality (nD)	S_{BET} (m^2 g^{-1})	Pore size (Å)	C_2H_2 uptake at 1 bar (mmol g^{-1})	C_2H_4 uptake at 1 bar (mmol g^{-1})	$Q_{st}(C_2H_2)$ at low loading (kJ mol^{-1})	S_{AE}	Temperature[a] (K)	Ref.
TIFSIX-14-Cu-i, 3D	425	3.6 × 3.6	3.78	1.41	54	229[b]	298	72
GeFSIX-2-Cu-i, 3D	467	4.5 × 4.5	3.9	2.2	42.6	67[b]	298	73
TIFSIX-2-Cu-i, 3D	685	5.1 × 5.1	3.9	2.1	46	55[b], 212.2[c]	298	47
SIFSIX-2-Cu-i, 3D	503	5.2 × 5.2	4.02	2.19	52.9	44.54[b], 41.01[c]	298	41
Ni-gallate, 3D	424	3.5 × 4.9	3.59	1.97	46	43.7[a]	298	74
NbOFFIVE-2-Ni-i, 3D	404	3.0 × 3.9	3.0	0.8	43	37.2[b]	298	75
NKMOF-1-Ni, 3D	382	5.8 × 5.8	2.72	2.14	58	1272.6[d], 30[c]	298	76
CPL-1, 3D	414	4.0 × 6.0	2.07	0.31	40.2	26.75[b]	298	77
M′MOF-3a, 3D	110	3.4 × 4.8	1.9	0.4	25	24.03[b], 34.17[c]	296	65
Mg-gallate, 3D	559	3.6 × 4.8	4.39	3.03	33	20.9[a]	298	74
UTSA-60a, 3D	484	4.8 × 4.0	3.12	2.05	36	16[b]	298	78
Co-gallate, 3D	475	3.7 × 5.0	3.88	3.37	47	15[b]	298	74
ELM-12, 2D	706	4.3 × 3.9	2.56	1.0	25.4	14.8[b]	298	79
APPT-Cd-ClO_4^-, 3D	205	11 × 11	1.75	0.44	28.6	14.71[c]	298	80
CPL-2, 3D	495	9.0 × 6.0	3.13	1.86	30.8	12[c]	298	77
pacs-CoMOF-2a	196	5.8[g], 6.6[g]	5.40	2.81	34.2	11.5[b]	298	81
UTSA-100a, 3D	970	4.3 × 4.3	4.27	1.66	22	10.72[b], 19.55[c]	296	82
SIFSIX-1-Cu, 3D	1178	8.0 × 8.0	8.5	4.11	30/37	10.63[b], 8.37[c]	298	41
UTSA-220, 3D	577	4.5 × 4.1; 2.1 × 5.0	3.4	2.53	29	10[b], 8.8[c]	298	83
SIFSIX-3-Zn, 3D	250	4.2 × 4.2	3.64	2.24	21/31	8.82[b], 13.72[c]	298	41
MUF-17, 3D	247[e]	3.1 × 3.5; 4.7 × 4.8	3.02	2.16	49.5	8.73[c]	293	84
JCM-1, 3D	550	3.9 × 12.5	3.34	1.56	36.9	8.1[c]	298	85
Sr-TCPE[f], 3D	NM[k]	5.2 × 4.3; 5.9 × 5.2	1.52	0.9	29	8[b]	298	86
ZJU-198a, 3D	343.1	3.6 × 4.1; 2.1 × 5.0	3.25	2.95	26.1	7.2[c]	298	87
UTSA-67a, 3D	1136.7	3.3 × 3.3	5.13	2.81	32	6[b]	298	88
SIFSIX-2-Cu, 3D	1881	10.5 × 10.5	5.38	2.02	26.3	6[b], 4.95[c]	298	41
CPL-5, 3D	523	11.0 × 6.0	3.01	1.84	31.3	6[b]	298	77
NBU-1, 3D	368	3.8[g]	3.64	2.07	38.3	5.9[c]	298	89
Ni-DCPTP, 3D	857	6.7[g], 10[g]	6.54	4.48	38.9	5.5[b]	298	90
SIFSIX-3-Ni, 3D	368	4.2 × 4.2	3.3	1.75	20.5	5.03[b], 5.98[c]	298	41
HUST-6, 3D	645.3	NA[h]	3.49	2.38	31.1	3.8[c]	298	91
Mg-MOF-74, 3D	927	11 × 11	8.37	7.45	41	2.18[b]	298	92
NOTT-300, 3D	1370	6.5 × 6.5	6.34	4.28	32	2.17[b], 2.3[c]	293	67
Fe-MOF-74, 3D	1350	11 × 11	6.8	6.1	46	2.08[b], 2.1[c]	318	66
Co-MOF-74, 3D	1018	11 × 11	8.17	7.02	45	1.7[b]	298	92
BUT-11, 3D	1233	11[g], 12.2[g]	7.14	3.44	20	NM[i]	298	93
Molecular sieves								
UTSA-300a[i], 2D	311	2.4 × 3.3	3.1	0.04	57.6	~10^4 [bj]	298	52
NCU-100a[i], 2D	358	3.4 × 3.4	4.57	0.32	60.5	7291.3[bj]	298	55
bnn-1-Ca-H_2O[i], 3D	210	3.4 × 3.4	2.2	0.16	NM[k]	6966.4[bj]	298	56
SIFSIX-14-Cu-i[i], 3D	612	3.4 × 3.4	1.8	0.6	40	6320[bj]	298	42
GeFSIX-14-Cu-i[i], 3D	424	3.0 × 3.0	4.1	0.76	43.6	1100[bj]	298	73
GeFSIX-dps-Cu,[il] 2D	382	1.8 × 2.6; 2.5 × 4.4	4.28	0.16	NM[k]	19[m]	298	94

[a] Temperatures used in the determination of uptakes and S_{AE}. [b] IAST selectivity at 1 bar for 1 : 99 (v/v) C_2H_2/C_2H_4. [c] IAST selectivity at 1 bar for 1 : 1 (v/v) C_2H_2/C_2H_4. [d] IAST selectivity at lowest C_2H_2 loading for 1 : 99 (v/v) C_2H_2/C_2H_4. [e] Determined from CO_2 isotherm recorded at 273 K. [f] TCPE = tetrakis((4-carboxyphenyl)ethylene). [g] Determined from Horvath–Kawazoe method or non-local density functional theory applied on N_2 isotherm at 77 K. [h] Pore size not defined due to post-synthetic metalation. [i] IAST selectivities are qualitative, because of molecular sieving. [j] Not applicable because of virial fits not conforming to stepped isotherms obtained at 298 and 273 K. [k] Not mentioned. [l] dps = 4,4′-dipyridylsulfide. [m] Uptake ratio at C_2H_2/C_2H_4 (0.1/0.9). S_{BET} = Brunauer–Emmett–Teller (BET) theory based surface areas from N_2 isotherm recorded at 77 K, unless otherwise mentioned.

reported for the four most widely studied binary C2 separations: C_2H_2/C_2H_4 (Table 1); C_2H_4/C_2H_6 (Table 2); C_2H_6/C_2H_4 (Table 3); C_2H_2/CO_2 and CO_2/C_2H_2 (Table 4). Whereas no attempt is made to analyse the data in Sections 4 and 5 focuses upon analysis of the structural and chemical driving forces for selective molecular recognition with emphasis upon two aspects: the types of binding sites in PCNs that are key to strong C2 separation performance; how, once a binding site is recognised and understood, crystal engineering approaches can be exploited to fine-tune first generation sorbents in order to further enhance selectivity and separation performance in the second generation of sorbents.

5. Crystal engineering of PCNs: in search of the optimal binding site

Section 4 tabulates some of the key structure and property parameters that are relevant to C2 LH separations (Tables 1–4). Now we address the various mechanisms that can drive

Table 2 Summary of the adsorption uptakes, selectivities and adsorption enthalpies (Q_{st}) for C_2H_4 and C_2H_6 in C_2H_4 selective sorbents (arranged from top to bottom aligned with a decreasing trend of selectivities)

Adsorbent, network dimensionality (nD)	S_{BET} ($m^2\ g^{-1}$)	Pore size (Å)	C_2H_4 uptake at 1 bar (mmol g^{-1})	C_2H_6 uptake at 1 bar (mmol g^{-1})	$Q_{st}(C_2H_4)$ at low loading (kJ mol^{-1})	$S_{C_2H_4/C_2H_6}$	Temperature[a] (K)	Ref.
UTSA-280, 3D	331	3.2 × 4.5; 3.8 × 3.8	2.5	0.098	34.1	>10[4 bc]	298	57
NUS-6(Hf)-Ag, 3D	1027	10, 17	2.02	1.35	56.5	106.3[d], 6[b]	298	95
ITQ-55, 3D	NM[e]	2.07 × 5.86	1.28	0.76	NM[e]	90[b]	303	96
Cu^I@UiO-66-$(COOH)_2$, 3D	320	4.1[f]	1.86	0.85	48.5	80.8[bg]	298	58
Co-gallate, 3D	475	3.69 × 4.95	3.37	0.31	44	52[b]	298	59
NOTT-300, 3D	1370	6.5 × 6.5	4.28	0.85	16	48.7[b]	293	67
Mg-gallate, 3D	559	3.56 × 4.84	3.03	0.26	39	37.3[b]	298	59
PAF-1-SO_3Ag, 3D	783	~8.0	4.06	2.23	106	27[b]	296	97
10 wt% Ag/CPL-2, 3D	12	7–11[f]	0.9	0.15	NM[e]	26.1[b]	298	98
Fe_2(*m*-dobdc), 3D	1295	12	7.0	6.0	55	25[b]	298	99
Ni-gallate, 3D	424	3.47 × 4.85	1.97	0.28	32	16.8[b]	298	59
NaETS-10, 3D	289	~8.0	1.7	1.3	NM[e]	14[b]	298	100
Fe-MOF-74, 3D	1350	11	6.28	5.10	47.5	13.6[b]	318	66
$ZnAtzPO_4$[h],[101] 3D	470	3.82 × 4.94	1.92	1.04	29.98	12.4[i]	298	102
(Cr)-MIL-101-SO_3Ag[j], 3D	1374, 1253	NM[e], 15–18[f]	3.26, 4.32	1.47, 1.22	63, 120	9.7[b], 16[b]	296, 303	103 and 104
1.6AgM-DS, 3D	846	NM[e]	3.37	0.94	59.2	9.5[b]	298	105
Co-MOF-74, 3D	1341	11	6.21	5.25	43.6	5.82[b]	318	106
Mg-MOF-74, 3D	927	11	7.4	6.4	42	5.6	296	92
Zeolite 5A, 3D	457–600	~5.0	2.45	1.72	37	4.5[b]	303	107
NUS-36, 3D	79.1	NM[e]	1.5	1.0	44	4.1[b]	298	108
HKUST-1, 3D	1500–2100	10, 14	7.20	6.03	39	3.6[b]	303	92
UiO-66-ADC	556	4.4	1.7	1.6	36	0.55[b]	298	108

[a] Temperatures used in the determination of uptakes and selectivities. [b] IAST selectivity at 1 bar for 1 : 1 (v/v) C_2H_4/C_2H_6. [c] IAST selectivities are qualitative, because of molecular sieving. [d] IAST selectivity at 0.01 bar for 1 : 1 (v/v) C_2H_4/C_2H_6. [e] Not mentioned. [f] Determined from Horvath–Kawazoe method applied on N_2 isotherm at 77 K. [g] Ascribed to the combined effect of π-complexation and size-sieving. [h] Atz = 3-amino-1,2,4-triazole. [i] Equilibrium-kinetic combined selectivity.[102] [j] Two consecutive reports on this sorbent document distinct values that are included using comma between them. S_{BET} = Brunauer–Emmett–Teller (BET) theory based surface areas from N_2 isotherm recorded at 77 K, unless otherwise mentioned.

selectivity (Sections 5.1–5.5) and present representative examples of binding sites (Section 5.6). That the availability of a new generation of highly selective PCN sorbents can enable C2 LH separation from multi-component gas mixtures is discussed in Section 5.7, in which the concept of SSST is explained.

The modularity of PCNs is key to their enormous diversity of pore size, structure and chemistry and their amenability to crystal engineering strategies once a parent sorbent or ''first generation'' sorbent is identified. In essence, the modularity of PCNs enables platforms or families of closely related PCNs to be generated in a systematic manner. Structure–function relationships can then be extrapolated as fine tuning of pore size and pore chemistry is feasible in a manner that is infeasible for other classes of porous physisorbents such as zeolites. For example, first generation HUMs such as SIFSIX-3-Zn and **SIFSIX-2-Cu-i** offered more than an order of magnitude improvement for CO_2/N_2[38] and C_2H_2/C_2H_4[41] capture, respectively. The level of control that can be exerted over the pore environment in such HUMs has in a short time enabled the second generation of HUMs to exhibit a further order of magnitude improvement in selectivity towards CO_2, C2 and C3 LHs.[42,166–168] Two main factors contribute to the benchmark performance of HUMs: tight-fit binding pockets (pore diameter ≤0.7 nm, sometimes ≤0.4 nm); strong electrostatics from inorganic anions, *e.g.* MoO_4^{2-}, SiF_6^{2-}, TiF_6^{2-} that serve as linkers/pillars.[28] In essence, ''lock-and-key'' molecular recognition can occur in a manner that mimics selective substrate binding in enzymes. More generally, for hard-to-separate C2 LH pairs (Fig. 2), LHs are physisorbed in PCN pores and can preferentially interact with binding sites through strong electrostatics, weak van der Waals forces, sorbate-unsaturated metal centre (UMC) interactions, hydrogen bonding (H-bonding) interactions or a combination thereof.[169] Binding site driven separations can be classified as equilibrium separations. Non-equilibrium separations are also possible with PCNs and would be driven by kinetics or molecular sieving.[10] Overall, thermodynamics, kinetic effects and steric considerations have all been shown to contribute as driving forces for adsorptive C2 separations by physisorbents.

The rapid increase in the frequency of reports of C2 separation and the ever-improving performance benchmarks mean that there is now a body of understanding about structure–function with respect to which types of binding sites are selective to a particular C2 LH. There is also realisation that a high density of strong and, ideally, single binding sites can lead to commensurate packing of sorbate molecules. When these features are both in play, a PCN is primed to exhibit strong C2 LH separation performance.

When one considers the full range of sorbents that have been studied, *i.e.* zeolites, activated carbons, mesoporous silica and PCNs (Fig. 3), preferred gas binding can be classified a being the consequence of one of five distinct mechanisms as follows: (a) size-exclusion guided molecular sieving; (b) thermodynamic equilibrium separation dictated by sorbent–sorbate binding; (c) differential diffusion to elicit kinetic *i.e.* non-equilibrium separation;[170] (d) conformational preference for one of the C2 LHs; (e) stimulus-induced separation, often facilitated by structural

Table 3 Summary of the adsorption uptakes, selectivities and adsorption enthalpies (Q_{st}) for C_2H_6 and C_2H_4 in C_2H_6 selective sorbents (arranged from top to bottom aligned with a decreasing trend of selectivities)

Adsorbent, network dimensionality (nD)	S_{BET} ($m^2\ g^{-1}$)	Pore size (Å)	C_2H_6 uptake at 1 bar (mmol g^{-1})	C_2H_4 uptake at 1 bar (mmol g^{-1})	$Q_{st}(C_2H_6)$ at low loading (kJ mol^{-1})	$S_{C_2H_6/C_2H_4}$	Temperature[a] (K)	Ref.
$Fe_2(O_2)$(dobdc), 3D	1073	7.6 × 7.6[b]	3.3	2.6	66.8	4.4[c]	298	60
UTSA-30, 3D	592	3.2 × 3.2[b]	2.1	2.1	30	3.8[c]	296	61
Qc-5-Cu-sql-β, 2D	240	3.3 × 3.3	1.8	0.8	37.6	3.4[c]	298	109
SBMOF-2, 3D	195	3.6 × 3.6[b]	2.8	2.7	32.3	3[c]	298	110
MAF-49, 3D	NM[d]	3.3 × 3.0	1.7	1.7	60	2.7[c]	316	68
ZJU-30, 3D	228	4.0 × 4.0; 5.6 × 5.6	2.1	2.0	29.7	2[c]	298	111
MUF-15, 3D	1130	8.5 × 3.5; 7.0 × 3.8	1.7	1.7	29.2	1.95[c]	298	112
Y-BTC, 3D	933	7.0 × 7.0	3.5	3.1	22	1.92[c]	298	113
PCN-250, 3D	1470	5.5 × 5.5; 9.6 × 9.6	5.2	4.2	23	1.9[c]	298	114
C-PDA-3[e], 3D	3160	NM[d]	6.57	5.10	22	1.9[c]	298	115
Eu-BTC, 3D	720	6.0 × 6.0	3.1	2.9	26	1.87[c]	298	113
IRMOF-8, 3D	1360	11.0 × 11.0	4.1	2.9	54	1.8[c]	298	116
NUM-7a, 3D	345	4.7 × 7.8	2.85	2.62	35.8	1.76[c]	298	117
CPM-733, 3D	1328.5	7.3 × 7.3	7.1	6.4	23.4	1.75[c]	298	118
ZIF-8, 3D	1844	3.5 × 3.5[e]; 11.6 × 11.6[f]	2.5	1.5	NM[d]	1.7[c]	293	119
ZIF-4, 3D	300	2.0 × 2.0[e]; 4.9 × 4.9[f]	2.3	2.2	NM[d]	1.7[c]	293	120
SBMOF-1, 3D	145	4.2 × 4.2	1.3	1.3	36.3	1.7[c]	298	110
Zn-atz-ipa, 3D	650	2.8 × 2.8[e]; 5.5 × 5.5[f]	1.8	1.8	45.8	1.7[c]	298	71
CPM-233, 3D	1598	6.8 × 6.8	7.4	6.5	27.3	1.64[c]	298	118
JNU-2, 3D	1219	3.7 × 3.7	4.1	3.6	29.4	1.6	298	121
ZIF-7, 3D	230	3.0 × 3.0[e]; 5.0 × 5.0[f]	1.9	1.8	NM[d]	1.6[c]	298	122
UTSA-38, 3D	1090	4.6 × 6.6	4.6	3.3	24.4	1.6[c]	296	123
[Ni(bdc)(ted)$_{0.5}$], 3D	1701	7.6 × 7.6; 5.1 × 3.7	5.0	3.4	21.5	1.6[c]	298	124
1a-tz, 3D	845	7.3 × 11.8	3.4	3.3	35	1.5[c]	298	125
MIL-142a, 3D	1580	7.0 × 7.0	3.8	2.9	27.3	1.5[c]	298	126
Azole-Th-1, 3D	983	10[f]	4.5	3.6	28.6	1.46[c]	298	127
Zn-PNMI, 3D	305	6.4 × 6.4[b]	1.6	1.7	23.5	1.42[g]	298	128
In-soc-MOF-1, 3D	1223	7.65 × 5.65; 10 × 10	4.0	3.7	28.4	1.4[h]	298	129
UTSA-33, 3D	660	5.4 × 6.5; 4.8 × 5.8	2.8	2.7	32	1.4[c]	296	130
UTSA-35, 3D	742	7.7 × 5.8	2.4	2.1	30	1.4[c]	296	131
Mn-PNMI, 3D	818	8.0 × 8.0[b]	2.8	2.0	24.5	1.38[g]	298	128
Cd-PNMI, 3D	264	7.6 × 7.6[b]	1.9	1.4	19.4	1.27[g]	298	128
TJT-100, 3D	890	8.7 × 11.6	3.7	3.4	29	1.2[c]	298	70

[a] Temperatures used in the determination of uptakes and selectivities. [b] Pore size determined using published crystal structures. [c] IAST selectivity at 1 bar for 1 : 1 (v/v) C_2H_6/C_2H_4. [d] Not mentioned. [e] Pore limiting diameter. [f] Largest pore opening. [g] IAST selectivity at 1 bar for 1 : 9 (v/v) C_2H_6/C_2H_4. [h] IAST selectivity at 1 bar for 1 : 15 (v/v) C_2H_6/C_2H_4. S_{BET} = Brunauer–Emmett–Teller (BET) theory based surface areas from N_2 isotherm recorded at 77 K, unless otherwise mentioned.

flexibility in a breathing or switching PCN. We highlight these modes through prototypal examples below.

5.1. Unsaturated metal centre (UMC) driven binding of unsaturated LHs

That an olefin such as C_2H_4 possesses unsaturated carbon–carbon double bonds makes it behave differently *versus* the competing paraffin *e.g.* C_2H_6 in terms of binding to metal centres. This difference is driven by the diffuse π-orbitals of C_2H_4 that can result in selective binding interactions with metal centres that line the pore surfaces of some families of PCNs.

PCNs can feature pore walls lined with coordinatively unsaturated metal centres (UMCs) and are therefore predisposed to preferentially bind to olefins over paraffins. Most typically, UMCs in as-synthesised PCNs are bonded to solvent molecules but activation results in removal of the solvent molecules and leads directly to the generation of UMCs that can interact with sorbates; interaction strength contingent on the relative electron densities of the UMCs.

Acetylene sorption studies on HKUST-1 conducted by B. Chen *et al.* resulted in structural determination of the C_2H_2 binding sites with Cu(II) UMCs (Fig. 6a).[171] HKUST-1 was earlier identified as being C_2H_4/C_2H_6 selective.[172] However, both C2 LHs are adsorbed by the Cu(II) UMCs in HKUST-1. The adsorption enthalpies (Q_{st}) are relatively low at *ca.* 32 kJ mol^{-1} with $[Q_{st}(C_2H_4) - Q_{st}(C_2H_6)]$ being <2 kJ mol^{-1}. Modest selectivity was thereby observed.[173] Nevertheless, the proof-of-principle established and a computational study[174] led Long's group to explore the UMC rich PCN family M-MOF-74 (also known as CPO-27-M, M_2(dhtp), or M_2(dobdc); M = Mg, Mn, Fe, Co, Ni, Zn; $dobdc^{4-}$ = 2,5-dioxido-1,4-benzenedicarboxylate) for C_2H_2/C_2H_4 and C_2H_4/C_2H_6 separations.[66,92] Fe-MOF-74 was found to exhibit the highest equimolar IAST selectivities of 2.08 and 13.6 for C_2H_2/C_2H_4 and C_2H_4/C_2H_6 respectively, in this family. The 1D hexagonal channels of *ca.* 11 Å are replete with a high density of UMCs that allow a limited degree of π-backbonding (Fig. 6b), despite the high-spin electronic configurations of transition metals in the respective M-MOF-74 analogues.[175] Topological and structural analogues of M-MOF-74, M_2(*m*-dobdc) MOFs (M = Mg, Mn, Fe, Co, Ni, Zn; *m*-$dobdc^{4-}$ = 4,6-dioxido-1,3-benzenedicarboxylate) were found to exhibit strong C_2H_4/C_2H_6 selectivity of ~25 in **Fe_2(*m*-dobdc)**.[99] Enhanced π-backbonding resulted in shorter M–C_{olefin} distances and was cited as the key factor behind enhanced performance.[176]

Table 4 Summary of the adsorption uptakes, selectivities and adsorption enthalpies (Q_{st}) for (a) C_2H_2 and CO_2 in C_2H_2 selective sorbents; (b) CO_2 and C_2H_2 in various CO_2 selective sorbents (both sections (a) and (b) arranged from top to bottom in decreasing trend of selectivities)

Adsorbent, network dimensionality (nD)	S_{BET} ($m^2\ g^{-1}$)	Pore size (Å)	C_2H_2 uptake at 1 bar (mmol g^{-1})	CO_2 uptake at 1 bar (mmol g^{-1})	$Q_{st}(C_2H_2)$ at low loading (kJ mol^{-1})	S_{AC}	Temperature[a] (K)	Ref.
(a) C_2H_2 selective adsorbents								
UTSA-300a, 2D	311	2.4 × 3.3	3.3	0.2	57.6	10[3 b]	298	52
ZJU-74a, 3D	694	3.6 × 3.8	3.83	3.08	44.5	36.5[b]	298	53
NKMOF-1-Ni, 3D	382	5.8 × 5.8	2.7	2.3	60.3	30[b]	298	76
CPL-1, 2D	571	4.0 × 6.0	1.9	0.07	42.5	26[c]	270	62
ZJU-196, 3D	NM[d]	5.1 × 5.1	3.7	0.4	39.2	25[e]	298	132
FeNi-M′MOF, 3D	383	4.15 × 4.27; 3.94 × 4.58	4.29	2.72	27	24[b]	298	54
$[Ni_3(HCOO)_6]_n$, 3D	289	4.3 × 4.3	2.4	1.6	40.9	22[b]	298	133
DICRO-4-Ni-i, 3D	398	6.2 × 6.6	1.9	1.0	37.7	18.2[e]	298	134
TCuCl, 3D	167	3.69 × 3.69	3.0	2.0	41	16.9[b]	298	64
pacs-CoMOF-2a	196	5.8,[g] 6.6[g]	5.40	2.81	34.2	13[b]	298	81
MIL-100(Fe), 3D	2300	5.5 × 8.6	5.3	2.5	65	12.5[e]	298	135
ZJU-40a, 3D	2858	10.2, 9.6 × 22.3	9.64	3.34	34.5	11.5[b]	298	136
Co-MOF, 3D	973	NM[d]	6.47	2.68	33	11[b]	298	137
TIFSIX-2-Cu-i, 3D	685	5.1 × 5.1	4.1	4.3	46	10[e]	298	47
JCM-1, 3D	550	12.5 × 3.9	3.3	1.7	36.9	10[b]	298	85
ZJUT-2a, 3D	350	3.2 × 3.2	3.4	2.2	41.5	10[b]	298	63
TCuBr, 3D	173	3.59 × 3.59	2.8	2.0	36.6	9.5[b]	298	64
UTSA-74a, 3D	830	8.0 × 8.0	4.8	3.2	31	9[b]	298	138
SNNU-150-Al, 3D	NM[d]	8.5[g]	4.33	1.98	29	7.27[b]	298	139
FJU-22a, 3D	828	7.1 × 7.1	5.1	5.0	23	7.1[f]	298	140
ZJU-60a, 3D	1627	4.4 × 5.4	6.7	3.3	17.6	6.7[f]	298	141
NTU-55, 3D	2300	10.4[g]	6.05	3.13	25	6.6[f]	298	142
UTSA-83a, 2D	70[h]	3.5 × 6.6	0.53	0.17	24.4	6.2[b]	298	143
MUF-17, 3D	247	4.7 × 4.8	2.7	2.2	49.5	6[b]	298	84
CPM-107op, 3D	319	NM[d]	4.35	1.55	37	5.7[b]	298	144
ZJNU-13, 3D	1352	6.8[g], 11.8[g]	5.28	3.92	33.5	5.64[b]	298	145
PCP-33, 3D	1248	11 × 20	5.4	2.6	27.5	5.6[e]	298	146
TCuI, 3D	250	3.66 × 3.66	2.2	1.6	38.4	5.3[b]	298	64
UPC-110, 3D	1384.3	6[g]	3.27	1.08	24.6	5.1[b]	298	147
JXNU-5, 3D	406	4.6[g], 6.7[g]	2.5	1.55	32.9	5[b]	298	148
Ag NP@Fe_2O_3@ Zn-MOF-74, 3D	936	7–10[g]	6.7	5.13	NM[e]	4.73[b]	293	149
SNNU-45, 3D	1006	4.5	5.98	4.33	40	4.5[b]	298	150
UTSA-220, 3D	577	4.5–5.5; 3.1–4.8	3.40	3.38	29	4.4[b]	298	83
FJU-89a, 3D	774	12 × 8	4.53	2.73	31	4.3[b]	296	151
FJU-90a, 3D	1572	5.4 × 5.1	8.0	4.6	25.1	4.3[b]	298	152
$Cu_2(ade)_2(PA)_2$, 3D	401	2 × 6	2.19	1.5	26.8	4.2[b]	298	153
ZJU-199a, 3D	987	5–7.5[g]	5.71	2.78	38.5	4[b]	296	154
Hex-Zn-MOF 1a, 3D	770.3	8.6[g], 9.8[g]	3.18	2.21	39	4[b]	298	155
mot-Cu(Br-BDC) MOF, 3D	303	4.2 × 4.7; 12 × 24.1	1.53	1.08	26.1	3.9[b]	298	156
Cu-CPAH, 3D	880	6–9[g]	5.88	3.93	35.4	3.6[b]	298	9
NBU-3-Mn/Fe, 3D	551	NM[d]	3.03	1.61	29	3.9[b]	273	157
UTSA-68a, 3D	1954	6.5 × 6.5; 7.5 × 9.5	3.13	1.77	25.8	3.4[b]	296	158
UPC-200(Al)-F-BIM, 3D	2212.8	7 × 11	6.2	2.5	20.5	3.15[b]	298	159
JNU-1, 3D	818	16.3 × 6.6	2.7	2.2	13	3[b]	298	160
Cu-tztp MOF 1a, 3D	798.9	5.4–8.6[g]	5.02	3.35	38.3	2.7[b]	298	161
Zn-MOF-74, 3D	1360	11 × 11	5.5	5.4	22.1	2[b]	298	138
ZJU-30a, 3D	228	4.0 × 4.0; 5.6 × 5.6	2.31	1.87	31.3	1.7[b]	296	158

Adsorbent, network dimensionality (nD)	S_{BET} ($m^2\ g^{-1}$)	Pore size (Å)	CO_2 uptake at 1 bar (mmol g^{-1})	C_2H_2 uptake at 1 bar (mmol g^{-1})	$Q_{st}(CO_2)$ at low loading (kJ mol^{-1})	S_{CA}[i]	Temperature[j] (K)	Ref.
(b) CO_2 selective adsorbents								
Tm(OH-bdc), 3D	923	6.3 × 9.3; 6.3 × 10.6	5.8	2.0	45.2	17.5[k]	298	162
CD-MOF-2, 3D	922	4.2 × 4.2, 7.8 × 7.8 (windows); 17 × 17 (cage)	2.7	2.0	67.2	16.6[k]	298	163
Mn(bdc)(dpe), 3D	535[l]	3.3 × 3.5	2.1	0.3	29	8.8	273	164
SIFSIX-3-Ni, 3D	368	4.2 × 4.2	2.7	3.3	50.9	7.7	298	47
CD-MOF-1, 3D	1094	4.2 × 4.2, 7.8 × 7.8 (windows); 17 × 17 (cage)	2.9	2.2	41.0	6.6[k]	298	163

Table 4 (*continued*)

Adsorbent, network dimensionality (nD)	S_{BET} (m^2 g^{-1})	Pore size (Å)	CO_2 uptake at 1 bar (mmol g^{-1})	C_2H_2 uptake at 1 bar (mmol g^{-1})	$Q_{st}(CO_2)$ at low loading (kJ mol^{-1})	S_{CA} [i]	Temperature [j] (K)	Ref.
$K_2[Cr_3O(OOCH)_6(4\text{-ethylpyridine})_3]_2[\alpha\text{-}SiW_{12}O_{40}]$, 0D	75 [l]	2.6 × 2.6 [m]; 3.5 × 3.5 [n]	2.4	0.5	*ca.* 39	4.8 [o]	278	165

[a] Temperatures used in the determination of uptakes and selectivities. [b] IAST selectivity at 1 bar for 1 : 1 (v/v) C_2H_2/CO_2. [c] Uptake ratio at 0.01 bar for 270 K measurements. [d] Not mentioned. [e] C_2H_2/CO_2 uptake ratio at 0.5 bar. [f] IAST selectivity at 0.15 bar for 1 : 1 (v/v) C_2H_2/CO_2. [g] Determined from Horvath–Kawazoe method applied on N_2 isotherm at 77 K. [h] Determined from CO_2 isotherm at 195 K. S_{BET} = Brunauer–Emmett–Teller (BET) theory based surface areas from N_2 isotherm recorded at 77 K, unless otherwise mentioned. [i] IAST selectivity at 1 bar for CO_2/C_2H_2 (1 : 1) mixture. [j] Temperatures used in the determination of uptakes and S_{AE}. [k] IAST selectivity at 1 bar for CO_2/C_2H_2 (1 : 2) mixture. [l] Surface area calculated from CO_2 195 K data. [m] Desolvated phase pore size. [n] MeOH solvated phase's pore size. [o] Uptake ratio at 1 bar. S_{BET} = Brunauer–Emmett–Teller (BET) theory based surface areas from N_2 isotherm recorded at 77 K, unless otherwise mentioned.

Olefin-selective binding in PCN physisorbents by UMCs has been reported in subsequent studies (Tables 1–4), including NKMOF-1-Ni,[76] NBU-1[89] and FeNi-M′MOF.[54] Two ultramicroporous MOFs, NKMOF-1-M, Cu[M(pdt)]$_2$ (M = Cu(II), Ni(II); pdt = pyrazine-2,3-dithiol) were introduced as C2 sorbents by Zhang's group in 2018. NKMOF-1-Ni was found to exhibit benchmark C_2H_2/C_2H_4 (1 : 99) selectivity of 1272.6 at low C_2H_2 coverage.[76] A combination of ultramicropores (5.75 Å) and square planar Ni(II) UMC sites might have been expected to be responsible for C_2H_2-selective binding and the $Q_{st}(C_2H_2)$ value of ~58 kJ mol^{-1}. However, analysis by dispersion-corrected density functional theory (DFT-D) and Grand Canonical Monte Carlo (GCMC) modelling attributed the strong C_2H_2 binding to hydrogen bonding (HC≡CH···S(MOF)) and π–π interactions between C_2H_2 and pyrazines from pdt ligands. Ni(II) or Cu(II) UMCs residing between the adjacent MS_4 units were deemed responsible for a second but weaker binding site for selective binding to C_2H_2 (Fig. 6c and d).

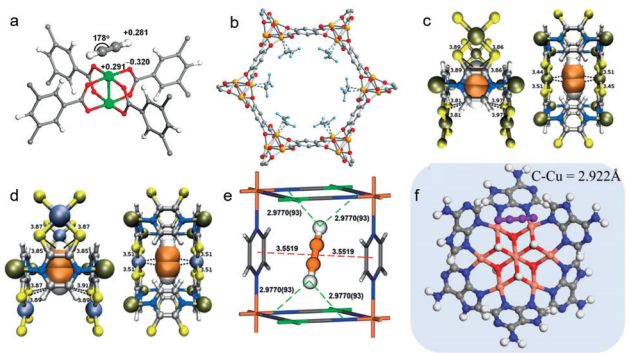

Fig. 6 Examples of binding of unsaturated C2 LHs to unsaturated metal centres in PCNs: (a) C_2H_2 in HKUST-1 as determined by DFT calculations;[171] (b) C_2D_4 in Fe-MOF-74 as determined by experimental NPD data;[66] (c) C_2H_2 in NKMOF-1-Ni as determined by DFT calculations;[76] (d) C_2H_2 in NKMOF-1-Cu as determined by DFT calculations;[76] (e) C_2D_2 in FeNi-M′MOF as determined by experimental NPD data;[54] (f) C_2H_2 in NBU-1 as determined by DFT-D calculations.[89] The labelled distances are measured in Å. (Reprinted with permissions from ref. 171, 66, 76, 54 and 89; copyright 2009, American Chemical Society; copyright 2012, American Association for the Advancement of Science; copyright 2018, Wiley-VCH Verlag GmbH & Co. KGaA, Weinheim; copyright 2020, Wiley-VCH Verlag GmbH & Co. KGaA, Weinheim; copyright 2019, American Chemical Society.)

B. Chen and colleagues also exploited two distinct binding modes in a Hofmann-type PCN FeNi-M′MOF, ([Fe(pyz)Ni(CN)$_4$], pyz = pyrazine) with Ni(II) UMCs and cyanide-linked ultramicropores of ~4.0 Å diameter. High C_2H_2/CO_2 IAST selectivity of ~24 was calculated for ambient conditions.[54] Uptake capacity of 4.54 mol L^{-1} during separation experiments from an equimolar C_2H_2/CO_2 mixture at 298 K and 1 bar makes FeNi-M′MOF second behind the benchmark sorbent UTSA-74 (4.86 mol L^{-1}).[138] DFT-D modelled structures and high-resolution neutron powder diffraction (NPD) experiments indicated preferential distribution of C_2D_2 between the two pyz rings through π–π stacking with multiple intermolecular $D^{\delta+}\cdots N^{\delta-}$ and $C^{\delta+}\cdots N^{\delta-}$ interactions between C_2D_2 and FeNi-M′MOF (Fig. 6e).

UMC driven LH selectivity was also studied by H.-C. Zhou's group, who reported the highest kinetic separation efficiency for C_2H_2/C_2H_4 in the ultramicroporous sorbent NBU-1, $(NH_4)\{Cu^{II}_3\cdot[Cu^{II}Cu^{I}_6(OH)_6(Ad)_6]_2\}\cdot xH_2O$ (Ad = adenine). The strong performance was attributed to its mixed-valence heptanuclear UMC-rich copper clusters and Lewis base adsorption sites. Spin-polarised DFT-D calculations revealed that, unlike the sorption mechanism shown by single Cu(II) UMCs, the C_2H_2 molecules in NBU-1 bind to the d-electron rich regions of two adjacent Cu(I) centres (Fig. 6f).[89] Other notable examples of UMC-driven C2 separations in PCNs include UTSA-74a,[138] ZJU-60a,[141] PCP-33.[146]

5.2. Hydrogen bonded binding sites

The presence of functional groups, particularly Lewis base moieties such as amines and[82,88,136] inorganic pillars such as SiF_6^{2-},[41,42,52,73,76] on the Connolly surfaces of PCN sorbents has evolved as a paradigm to enhance C2 adsorption capacity and selectivity. As mentioned earlier, Kitagawa's group introduced the prototypal C_2H_2 selective sorbent in 2005, CPL-1 *i.e.* [Cu$_2$(pzdc)$_2$(pyz)] (pzdc = pyrazine-2,3-dicarboxylate). This low-surface area (*ca.* 571 m^2 g^{-1}) PCN exhibited uptakes consistent with strong C_2H_2/CO_2 selectivity (uptake ratio ~26 at 270 K).[62] Maximum entropy method (MEM)/Rietveld analysis of CPL-1 revealed C_2H_2 molecules residing at periodic distances from one another sustained by H-bonding between two non-coordinated oxygen atoms of pzdc ligands and each of the two H-atoms of C_2H_2 (Fig. 7a). The C_2H_2-specific sorption of CPL-1 was attributed to a combination of electrostatic attractions and electron delocalization effects between C_2H_2(C–H)

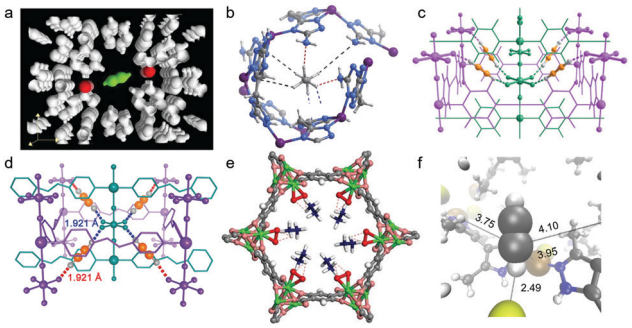

Fig. 7 Illustrations of preferential H-bonded binding sites: (a) C_2H_2 in CPL-1 as determined by MEM/Rietveld analysis;[62] (b) C_2H_6 in MAF-49 as determined by DFT calculations;[68] (c) C_2H_2 in **SIFSIX-2-Cu-i** as determined by DFT-D calculations;[41] (d) C_2D_2 in **SIFSIX-14-Cu-i** as determined by experimental NPD data;[42] (e) C_2D_6 in $Fe_2(O_2)$(dobdc) as determined by experimental NPD data;[60] (f) C_2H_2 in TCuCl as determined by simulated annealing.[64] (Reprinted with permissions from ref. 62, 68, 41, 42, 60 and 64: copyright 2005, Springer Nature; copyright 2015, Springer Nature; copyright 2016, American Association for the Advancement of Science; copyright 2017, Wiley-VCH Verlag GmbH & Co. KGaA, Weinheim; copyright 2018, American Association for the Advancement of Science; copyright 2020 Wiley-VCH Verlag GmbH & Co. KGaA, Weinheim.)

and O–C(sorbent), an example of a guest 'confinement effect' to elicit stoichiometric C_2H_2 trapping. O-donor based selective C_2H_2 binding has also been seen in a number of recent reports, including FJU-22a,[140] TJT-100[70] and JCM-1.[85] In a related approach, amine introduction into ultramicropores in the prototypal AUM MAF-49, [Zn(batz)] (H_2batz = bis(5-amino-1*H*-1,2,4-triazol-3-yl)methane), resulted in one of the first reports of C_2H_6 selective sorption from C2 LH mixtures.[68] Strong C_2H_6 binding was manifested by high $Q_{st}(C_2H_6) \sim 60$ kJ mol^{-1} and the then benchmark C_2H_6/C_2H_4 selectivity was attributed to three strong C–H···N hydrogen bonds and three weak C–H···N electrostatic interactions (Fig. 7b).

A key discovery concerning purification of C_2H_4 was realised by H. Xing, B. Chen and Zaworotko's collaborative studies on HUMs which included both non-interpenetrated and interpenetrated HUMs (i-HUMs). They reported a design and property breakthrough in terms of pore size and pore chemistry.[41] From the sorbent design perspective, the HUMs studied each exhibit pores lined with hexafluorosilicate (SIFSIX) anions. From the property perspective, whereas the previous benchmark for C_2H_2/C_2H_4 selectivity exhibited an IAST selectivity of only 2.08 (Table 1),[66] this family of HUMs, which comprises M(II)–$N_{heterocycle}$ **sql** topology nets pillared by SIFSIX anions, resulted in more than an order of magnitude improvement in selectivity (1 : 99 C_2H_2/C_2H_4 IAST selectivity at 1 bar, $S_{AE} \sim 44.54$) for the prototypal i-HUM, **SIFSIX-2-Cu-i**, a sorbent that exhibits 2-fold interpenetration. This exceptional selectivity was driven by exposed SIFSIX moieties that enable CH···F bonding to both sides of C_2H_2 molecules (Fig. 7c). More importantly, C_2H_2 binding was found to be markedly different in related materials such as **SIFSIX-1-Cu**, [Cu(SiF_6)($bpy)_2$], which adsorbed 8.5 mmol g^{-1} of C_2H_2 at 298 K and 1 bar, *ca.* twice that of the larger-pore HUM **SIFSIX-2-Cu** [Cu(SiF_6)($py_2C_2)_2$; py_2C_2 = 4,4′-dipyridylacetylene].[41] However, the latter HUMs are just moderately C_2H_2 selective over C_2H_4 ($S_{AE} \sim 10.6$ and 6.0, respectively; Table 1) whereas **SIFSIX-2-Cu-i** binds C_2H_2 strongly with $Q_{st}(C_2H_2) = 52.9$ kJ mol^{-1}, a consequence of the aforementioned H-bonding interactions. Dynamic column breakthrough (DCB) experiments conducted upon **SIFSIX-2-Cu-i** yielded high-purity ethylene with C_2H_2 concentrations as low as 2 ppm. Substitution of linker 2 (py_2C_2) in **SIFSIX-2-Cu-i** with 4,4′-azopyridine (14) afforded the second generation HUM variant **SIFSIX-14-Cu-i**, which exhibits trace C_2H_2 capture from a 1 : 99 C_2H_2 : C_2H_4 mixture thanks to near-ideal molecular sieving.[42] Typical of a molecular sieve, the record high IAST selectivity of 6320 at 1 bar (1 : 99 C_2H_2/C_2H_4) and doubling of C_2H_4 production capacity compared to **SIFSIX-2-Cu-i** represented a significant breakthrough, more than an incremental improvement. Each adsorbed C_2D_2 interacts with two SiF_6^{2-} anions from different interpenetrating nets through cooperative C–D···F H-bonds, the length of these bonds (1.921 Å) being smaller than those in **SIFSIX-2-Cu-i** (2.015 Å). These distances are reflective of stronger H-bonding interactions in the narrower-pore azopyridine HUM (Fig. 7d).

The microporous MOF $Fe_2(O_2)$(dobdc) was recently reported by J. Li and B. Chen's group and binds ethane with a high $Q_{st}(C_2H_6) \sim 67$ kJ mol^{-1}, leading to $S_{C_2H_6/C_2H_4}$ of 4.4 for an equimolar mixture at 298 K and 1 bar. Breakthrough experiments using an equimolar mixture of C_2H_6 and C_2H_4 by a single DCB column of $Fe_2(O_2)$(dobdc) yielded polymer-grade C_2H_4 as effluent, with 99.99% purity. Prepared by addition of O_2 to Fe_2(dobdc), $Fe_2(O_2)$(dobdc) features η^2-bound peroxo–Fe(II) sites, and NPD analysis recorded at 7 K indicated that these sites couple with electronegative surface oxygen distributions to engage in close contacts with $-CH_3$ groups of the adsorbed ethane molecules (Fig. 7e). A downside of Fe_2(dobdc) and $Fe_2(O_2)$(dobdc) is that they are air sensitive and must be handled in a moisture-free environment.

The benchmark C_2H_2 selectivity of i-HUMs such as **SIFSIX-2-Cu-i**,[41] **TIFSIX-2-Cu-i**,[47] GeFSIX-2-Cu-i,[73] NbOFFIVE-2-Ni-i,[75] **SIFSIX-14-Cu-i**,[42] TIFSIX-14-Cu-i,[72] GeFSIX-14-Cu-i[73] is credited to cooperative C–H···F hydrogen bonding between acetylene and the inorganic pillars. Halide ligands bound to Cu(I) in an isostructural family of ultramicroporous MOFs, TCuX (X = Cl, Br, I), [Cu(TMBP)X] (TMBP = 3,3′,5,5′-tetramethyl-4,4′-bipyrazole) were also found to exhibit strong C_2H_2 binding driven by C–H···X H-bonds (Fig. 7f).[64] A new benchmark for C_2H_2/CO_2 separation selectivity was found for TCuCl with relative selectivities consistent with the H-bonding strength: C–H···Cl (2.49 Å) < C–H···Br (2.57 Å) < C–H···I (2.80 Å).

5.3. Olefin-π complexation to Ag(I) and Cu(I)

The first metal–olefin complex, platinum(II)–ethylene, Zeise's salt, can be traced back to 1827.[177] Dewar, Chatt and Duncanson developed[178] a π-back bonding model for such complexation (Fig. 8) which can be exploited to generate olefin-selective sorbents. Among transition metals that exhibit π-complexation with C_2H_4, Ag is the most widely used followed by Cu. Rather than physisorption, the binding here is regarded as reactive

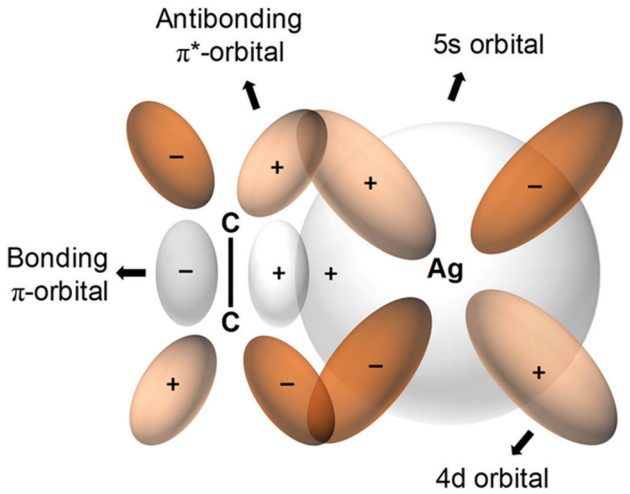

Fig. 8 π-Complexation between an olefin such as C_2H_4 and Ag(I) ions[182] results in enhanced C_2H_4/C_2H_6 selectivities in several PCNs. (Reprinted with permission from ref. 183: copyright 2018, American Chemical Society.)

absorption *via* gas/liquid contact.[179] Regardless of the generality of this approach, it was adjudged inefficient because of the weak contact between LH gases and liquid absorbents.[180] In 2008, the nonporous compound, $Ag_2[Cr_3O(OOCC_2H_5)_6(H_2O)_3]_2$-[α-$SiW_{12}O_{40}$], which is comprised of 2D layers of polyoxometalates and macrocations, exploited C_2H_4 complexation to exhibit strong C_2H_4/C_2H_6 sorption selectivity (uptake ratio >100 at 298 K and 1 bar).[179] Silver-exchanged zeolite A (AgA) revealed size-selective molecular sieving of C_2H_6 and this "absolute" C_2H_4 selective sorbent was shown to be recyclable through vacuum and/or temperature swing experiments.[181] Porous aromatic frameworks (PAFs) were also used to demonstrate this strategy in PAF-1-SO_3Ag ($S_{C_2H_4/C_2H_6}$ = 27). Sorption/selectivity experiments with PAF-1 ($S_{C_2H_4/C_2H_6}$ = 0.7) and PAF-1-SO_3H ($S_{C_2H_4/C_2H_6}$ = 0.88) underscored the profound role of Ag-complexation behind the enhanced C_2H_4 selectivity.[97] B. Chen and S. Ma's groups used this complexation strategy in mesoporous MIL-101, (Cr)-MIL-101-SO_3Ag, leading to $S_{C_2H_4/C_2H_6}$ = 16 *versus* the control variant, (Cr)-MIL-101-SO_3H = 1.15.[103,104] Zhao and co-workers further pursued this approach on a microporous Hf MOF, NUS-6(Hf)-Ag ($S_{C_2H_4/C_2H_6}$ = 6) *vs.* that of NUS-6 ($S_{C_2H_4/C_2H_6}$ = 0.9).[95] Related reports include a study of CPL-2 ($S_{C_2H_4/C_2H_6}$ = 1.4) modified to 10 wt% Ag/CPL-2 ($S_{C_2H_4/C_2H_6}$ = 26.1)[98] and 1.6AgM-DS.[105] Qian's group recently extended this approach to the Cu(I) chelated physisorbent Cu^I@UiO-66-$(COOH)_2$, which combines olefin complexation with controlled pore size to enable molecular sieving exclusion of C_2H_6 and $S_{C_2H_4/C_2H_6}$ of 80.8.[58]

5.4. Flexible coordination networks

Several flexible PCNs with gated pores have been reported to achieve efficient separation of C2 LHs *via* gas-specific induced gate-opening. Unlike the canonical Langmuir model driven type I isotherms in rigid physisorbents, flexible PCNs are characterised by characteristic gating isotherms with five distinct isotherm types (F-I to F-V).[184] A 'step' refers to a sudden increase in uptake at a threshold pressure that results from flexibility or a phase change of the adsorbent. Flexible PCNs that feature stepped type F-IV isotherms, which transform from non-porous to porous phases, can offer higher working capacity *vs.* rigid PCNs.[185] The type F-IV C2 isotherms exhibited by **ZIF-7** [$Zn(bim)_2$, bim^- = benzimidazolate] at ambient temperature feature lower gate-opening pressure for C_2H_6 than C_2H_4, making it an early example of an ethane-selective PCN (Table 3).[122] Leveraging this C_2H_6 selectivity, C_2H_6/C_2H_4 separation performance was confirmed by equimolar binary DCB experiments. That C_2H_6 adsorption revealed a more exothermic profile *versus* C_2H_4 adsorption over the entire C2 sorption coverage can explain why gate opening occurred more readily for C_2H_6. With respect to sorbent–sorbate binding, C_2H_6 is thought to maximize van der Waals (vdW) interactions with the Connolly surface thanks to its 3-fold rotational symmetry matching that of **ZIF-7** ultramicropores (pore limiting dimeter: 3.0 Å; largest pore opening: 5.0 Å) (Fig. 9a).[122,186] Whereas H-bonding was identified as the key factor in realising C_2H_2 selectivity over CO_2 in CPL-1 (Section 5.2),[62] this sorbent exhibited an abrupt step increase in its C_2H_4 adsorption isotherm at 273 K and ~2 bar. No step was noticed for C_2H_6 at 273 K, despite subjecting it to an elevated pressure of ~10 bar.[187] DCB experiments at 8 bar and 273 K demonstrated effective C_2H_4/C_2H_6 separation. Optimised geometries of C_2H_4 and C_2H_6 were consistent with the C_2H_2 binding modes earlier obtained *via* MEM/Rietveld analysis.[62] An allosteric pore-opening mechanism for C_2H_4 selective sorption over C_2H_6 was observed in the dehydrated and guest-free, nonporous phase of the PCN $[Co(vttf)]_n$ {$vttf^{2-}$ = 2,2′-[1,2-bis(4-benzoate)-1,2-ethanediylidene]bis-1,3-benzodithiole}.[188] The PCN structure is crosslinked

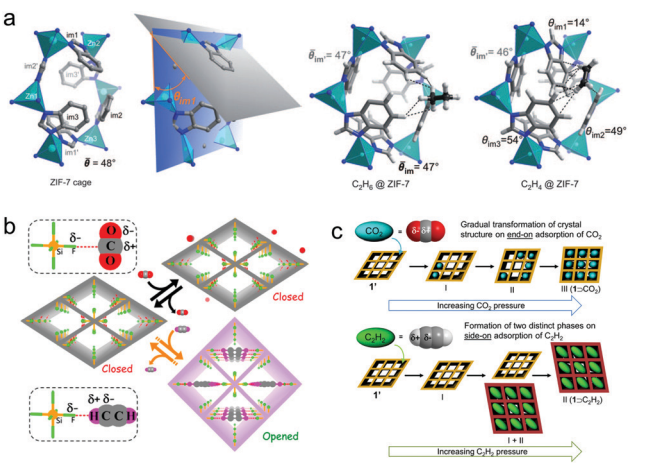

Fig. 9 (a) Left: the optimised structure of the **ZIF-7** cage entrance and a schematic illustration of the θ_{Im1} parameter (the angle between a plane accommodating Zn1, Zn2 and Zn3 atoms and a plane of the Im1 benzimidazole moiety), adsorption complexes of C_2H_6 and C_2H_4 in the window of **ZIF-7** (average values of θ are presented when deviation between the individual values is minor).[186] Schematic adsorption mechanisms showing distinct dynamic behaviour for CO_2 and C_2H_2 adsorption in (b) UTSA-300a;[52] (c) [Mn(bdc)(dpe)].[164] Reprinted with permissions from ref. 186, 52 and 164: (reprinted with permissions from ref. 52, 164 and 186: copyright 2011 Wiley-VCH Verlag GmbH & Co. KGaA, Weinheim; copyright 2017, American Chemical Society; copyright 2016, American Chemical Society).

by the coordination of tetrathiafulvalene sulphur atoms to the axial sites of $Co_2(COO)_4$ paddlewheels. Whereas $[Co(vttf)]_n$ is unresponsive to ethane, exposure to ethylene induces a cooperative transition driven by coordination to Co(II). This in turn displaces the tetrathiafulvalene linkers to afford an open architecture. Once open, $[Co(vttf)]_n$ co-adsorbs both C2 gases, resulting in only modest selectivity. Co-adsorption of multiple components represents an oft-encountered issue for flexible PCNs in separating C2 LH mixtures, especially when high purity in the sorbed phase is required.

Despite the prevalence of 3D HUMs for studies on C2 LHs, the 2D layered PCN $[Zn(SiF_6)(dps)_2$; dps = 4,4′-dipyridylsulfide], UTSA-300a, is the current benchmark for C_2H_2/CO_2 and C_2H_2/C_2H_4 separation by a physisorbent thanks to its trace C_2H_2 capture performance.[52] Interactions between pyridyl H atoms *ortho* to nitrogen and the SiF_6^{2-} anions induce a tilting of the coordinated pyridyl rings. This blocks the pores of UTSA-300a from CO_2 and/or C_2H_4 (Fig. 9b, top). However, C–H···F bonds drive cooperative gate opening upon exposure to C_2H_2 with pressures above ~0.2 bar (at 298 K). C_2H_2 molecules bridge two diagonally opposite SiF_6^{2-} (Fig. 9b, bottom). C_2H_2 selective flexibility driven by these binding modes was in agreement with the stepped gate opening isotherms observed exclusively for C_2H_2. Equimolar C_2H_2/C_2H_4 and C_2H_2/CO_2 DCB experiments with UTSA-300a yielded C_2H_4 and CO_2, respectively, with both effluents of purity >99.9%, a rarity among C2 purifying sorbents. Two recent follow-up studies were reported for NCU-100a[55] and GeFSIX-dps-Cu.[94] Both sorbents exhibited molecular sieving and C_2H_2 selective sorption to afford high-purity C_2H_4 as effluent from 1 : 99 and equimolar (v/v) mixtures. Each sorbent exhibited stepped isotherms, suggesting that the combination of molecular sieving and C–H···F H-bonds might be of broad relevance for C2 LH separations.

The 2-fold interpenetrated 3D PCN [Mn(bdc)(dpe)] (bdc = 1,4-benzenedicarboxylate, dpe = 1,2-di(4-pyridyl)ethylene) was observed to undergo sudden gate opening for CO_2 and not for C_2H_2, implying CO_2 sorption selectivity over C_2H_2, at 273 K. To examine the mechanism of this CO_2 selective gated sorption (Fig. 9c), [2+2] photodimerization on Mn(bdc)(dpe) was conducted. The photodimerised variant, $[Mn_2(bdc)_2(rctt\text{-tpcb})]$ (*rctt*-tpcb = region-*cis*,*trans*,*trans*-tetrakis(4-pyridyl)cyclobutane), exhibited no CO_2 selectivity. Other PCNs that rely upon flexibility as the primary mechanism for selective LH capture include M′MOF-3a[65] and ELM-12.[79] Both of these flexible PCNs are selective for C_2H_2 over C_2H_4 and offer 1 : 99 C_2H_2/C_2H_4 selectivities >15 (Table 1).

5.5. Pore size control

Non-equilibrium physisorption from kinetic separation and molecular sieving[170] relies upon the diffusivity difference of gas molecules. Relative pore sizes typically dictate separation performance. The profound impact that pore size/chemistry can exert on adsorption properties was exemplified by varying the pore size and degree of interpenetration in a series of **pcu** MFSIX HUMs (see Section 5.2 for details). In particular, thanks to near-ideal molecular sieving in **SIFSIX-14-Cu-i**, *i.e.* C_2H_2 trapped through cooperative C–H···F H-bonding (2.015 Å for

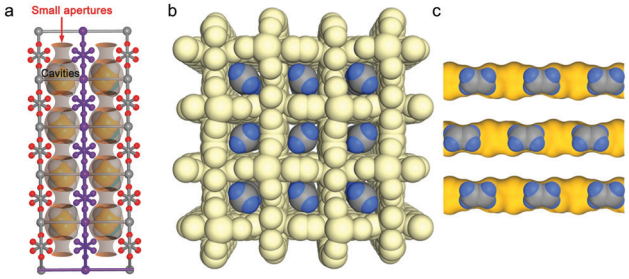

Fig. 10 Schematic illustrations of pore size-controlled uptake of (a) C_2H_2 in **SIFSIX-14-Cu-i**;[42] (b and c) C_2H_4 in UTSA-280.[57] (Reprinted with permissions from ref. 42 and 57: copyright 2017, Wiley-VCH Verlag GmbH & Co. KGaA, Weinheim; copyright 2018, Springer Nature.)

C_2H_2, Fig. 10a), this HUM was reported as the benchmark sorbent for C_2H_2 capture (volumetric uptake, 58 cm^3 cm^{-3}) at 0.01 bar.[42] Furthermore, **SIFSIX-14-Cu-i** recorded benchmark C_2H_4 productivity of 87.5 mmol g^{-1} per cycle, effluent C_2H_4 purity >99.99% and simultaneous production of high purity C_2H_2 (97%) *via* an energy-efficient desorption at 338 K. A follow-up study on the variants NCU-100a[55] and GeFSIX-dps-Cu[94] found record-high C_2H_4 purification performance by trace C_2H_2 capture which was also attributed to molecular sieving.

Another example of near-ideal molecular sieving was exemplified by UTSA-280, the easily scalable and low-cost MOF Ca(squarate).[57] Unlike most of the MOFs that exhibit variable pore size owing to linker dynamics, UTSA-280 features 1D rigid pore channels (aperture sizes: 3.2 × 4.5; 3.8 × 3.8 in Å, Fig. 10b) and behaves as an ideal size-selective molecular sieve to exclude C_2H_6 from C_2H_4 even from 1 : 99 trace gas mixtures. Ultramicropore windows in UTSA-280, with a cross-sectional area of *ca.* 14.4 $Å^2$ (Fig. 10c), fit right between the minimum cross-sectional areas of the completing sorbates: C_2H_4 (13.7 $Å^2$) and C_2H_6 (15.5 $Å^2$), thus explaining the observed exclusion of C_2H_6.

5.6. Case studies for selective binding sites in C2 sorbents.

5.6.A. C_2H_2/C_2H_4 separation. Acetylene/ethylene separation is one of the most widely studied C2 LH separations using PCNs (Table 1). C_2H_2 binding modes that promote efficient C_2H_2/C_2H_4 selectivities (S_{AE}) at ambient conditions were covered above and are exemplified by CPL-1,[62] HKUST-1,[171] **SIFSIX-2-Cu-i**,[41] UTSA-300a,[52] **SIFSIX-14-Cu-i**;[42] NKMOF-1-Ni,[76] NKMOF-1-Cu,[76] TCuCl,[64] FeNi-M′MOF[54] and NBU-1.[89] The full range of high-performing PCN sorbents includes NOTT-300, reported by Schröder's group in 2012. NOTT-300 is $[Al_2(OH)_2(L)]$ (H_4L = biphenyl-3,3′,5,5′-tetracarboxylic acid) and selectively binds CO_2 and SO_2.[189] In 2015, the same group established that intermolecular dipole interactions with M–OH groups, aromatic –CH and phenyl rings (Fig. 11a) result in weak interactions with unsaturated LHs such as C_2H_2 and C_2H_4 to exhibit C_2H_2/C_2H_4 and C_2H_4/C_2H_6 equimolar (v/v) DCB separations.[67] The multiple-site cooperative binding mechanism suggested by DFT-D was in agreement with experimental results obtained from inelastic neutron scattering (INS) spectra, quasi-elastic neutron scattering (QENS) spectra, neutron diffraction and synchrotron X-ray diffraction.

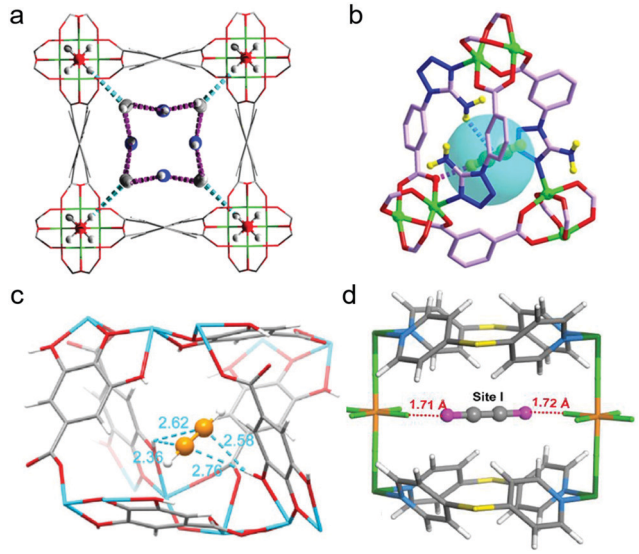

Fig. 11 Preferential C_2H_2 binding sites in C_2H_2/C_2H_4 selective adsorbents: (a) NOTT-300, as determined by DFT-D modelling;[67] (b) UTSA-100a, as determined by DFT-D calculations;[82] (c) Mg-gallate, as determined by NPD experiments;[74] (d) NCU-100a, as determined by Rietveld refinement.[55] (Reprinted with permissions from ref. 67, 82, 55 and 74: copyright 2019, Wiley-VCH Verlag GmbH & Co. KGaA, Weinheim; copyright 2015, Springer Nature; copyright 2020, American Chemical Society; copyright 2014, Springer Nature.)

The microporous MOF [Cu(ATBDC)] (ATBDC = 5-(5-amino-1*H*-tetrazol-1-yl)-1,3-benzenedicarboxylate), UTSA-100a, was reported by B. Chen's group to efficiently remove C_2H_2 from 1 : 99 C_2H_2/C_2H_4 mixtures. C_2H_2 binding was studied by DFT-D calculations. One C_2H_2 molecule sits inside the small cage that links adjacent channels. This C_2H_2 binding mode, which resulted in an experimental $Q_{st}(C_2H_2)$ of ~31.3 kJ mol^{-1}, is an outcome of multiple supramolecular interactions of C_2H_2 with the pore wall of UTSA-100a (Fig. 11b). The weak basicity of aromatic $-NH_2$ groups is complementary to weakly acidic C_2H_2 molecules (pK_a = 25).[190] Owing to its lower acidity, C_2H_4 (pK_a = 44[190]) does not interact as strongly with the $-NH_2$ moieties.

The aperture size of the 3D isostructural family of metal-gallate MOFs (M-gallates; M = Ni(II), Mg(II), Co(II)) ranged from 3.69 Å to 3.47 Å[74] and S_{AE} is highest for Ni-gallate. NPD studies of C_2D_2 and C_2D_4 loaded Mg-gallate phases revealed that C_2D_2 molecules locate at the centre of the Mg-gallate pore sustained by symmetrical $Cd^{\delta-}\cdots H^{\delta+}O^-$ interactions (C···H–O = 2.36–2.76 Å) from –OH groups of two neighbouring gallates (Fig. 11c). The strong C_2H_2 binding in Ni-gallate ranked it just after **SIFSIX-14-Cu-i**, resulting in ethylene productivity of 85.6 mol L^{-1} from a 1 : 99 C_2H_2/C_2H_4 mixture.

Metal-node substitution of the current C_2H_2/C_2H_4 and C_2H_2/CO_2 benchmark physisorbent, UTSA-300a (Section 5.4),[52] afforded the isostructural variant NCU-100a, $[Cu(SiF_6)(dps)_2]$.[55] UTSA-300a possesses internal cages of 3.5 × 3.9 × 4.1 Å^3 that are inaccessible to C_2H_2 molecules until dps linker rotation occurs at the C_2H_2 gate opening pressure of ~0.2 bar at 298 K. On the contrary, elongated Cu–F bonds increase the pore cavities in NCU-100a thanks to Jahn–Teller distortion and result in expanded internal cages of 3.6 × 4.3 × 4.2 Å^3. The cages can selectively accommodate C_2H_2 at low pressure. Rietveld refinement of the PXRD pattern recorded *in situ* for C_2H_2 saturated NCU-100a revealed C_2H_2 molecules trapped in cage-like pores with dual C–H···F hydrogen bonds between C_2H_2 terminal F atoms of different SiF_6^{2-} units. C–H···F bond lengths of 1.71 and 1.72 Å were observed (Fig. 11d). C_2H_2-specific binding and molecular sieving enabled NCU-100a to achieve C_2H_2 uptake improvement (~4.57 mmol g^{-1}) *vs.* UTSA-300a (~3.1 mmol g^{-1}) and a high effluent C_2H_4 productivity of 14.9 mmol g^{-1}. Remaining examples of C_2H_2/C_2H_4 selective physisorbents are listed by decreasing S_{AE} in Table 1.

5.6.B. C_2H_4/C_2H_6 separation. Olefin/paraffin C_2H_4/C_2H_6 separation is probably the most studied LH separation with early studies centred on ion exchanged zeolites and weak chemisorbents.[180,191] In Sections 5.1 and 5.5, Fe-MOF-74[66] and UTSA-280[57] were detailed, respectively. Now we highlight three more examples of PCNs which exhibit high C_2H_4/C_2H_6 selectivity: **Fe$_2$(*m*-dobdc)**,[99] Co-gallate[59] and ZnAtzPO$_4$.[102] Long and co-workers suggested that increased charge densities at the coordinatively unsaturated M(II) sites (M = Mg, Mn, Fe, Co, Ni, Zn) in M_2(*m*-dobdc) MOFs resulted in enhanced $S_{C_2H_4/C_2H_6}$ *vs.* most other physisorbents, including the dobdc analogue M_2(dobdc), also known as M-MOF-74.[99] Among the isostructural variants, **Fe$_2$(*m*-dobdc)** recorded $S_{C_2H_4/C_2H_6}$ ~ 25 at 1 bar for an equimolar (v/v) mixture and a high C_2H_4 saturation uptake of ~7 mmol g^{-1}. *In situ* single crystal X-ray characterization of C_2H_4 binding in the isostructural variant **Co$_2$**(*m*-dobdc) revealed that the C_2H_4/C_2H_6 selectivity enhancement *vs.* Co-MOF-74 is likely an outcome of stronger metal–olefin interactions induced by higher charge densities at the soft Co(II) UMCs with weak π-basicity (Fig. 12a).

The M-gallates (M = Ni(II), Mg(II), Co(II)) detailed in Section 5.6.A (Fig. 11c) were also studied for C_2H_4/C_2H_6 selectivity and separation.[59] The 3D interconnected zigzag channels of these ultramicroporous MOFs feature a narrow range of aperture sizes ~3.47–3.69 Å, suitable for molecular sieving based upon selective entry of C_2H_4 (3.28 × 4.18 × 4.84 Å^3) over C_2H_6 (3.81 × 4.08 × 4.82 Å^3). Co-gallate, with $S_{C_2H_4/C_2H_6}$ ~ 52 and a C_2H_4 saturation uptake of 3.37 mmol g^{-1} at 298 K and 1 bar, performed well in equimolar (v/v) DCB experiments. NPD studies on Mg-gallate·0.485C_2D_4 at 200 K revealed C_2D_4 to be encircled by Mg(II) ions and two adjacent gallates. Cooperative interactions between C(δ^-) of C_2D_4 and H(δ^+) from –OH of the two parallel gallates (C···H–O = 2.28–2.68 Å) (Fig. 12b) play a key role in sorbent–sorbate binding. Furthermore, C–D···O interactions between C–D of C_2D_4 and gallate ligands further augments binding.

To lower the adsorption enthalpy of sorbent regeneration, the use of a phosphate anion in the pillared ultramicroporous MOF ZnAtzPO4[101] (Atz = 3-amino-1,2,4-triazole) enabled C_2H_4/C_2H_6 (1 : 1, v/v) DCB separation performance with low $Q_{st}(C_2H_4)$ of *ca.* 30 kJ mol^{-1}.[102] That ZnAtzPO4 traps C_2H_4 and restricts the diffusion of C_2H_6 resulted in an equilibrium-kinetic combined selectivity of 32.4 as reported by H. Xing *et al.* The C_2H_4 binding mechanism was studied by first-principles DFT-D calculations, which revealed that $ZnAtzPO_4$ provides two distinct

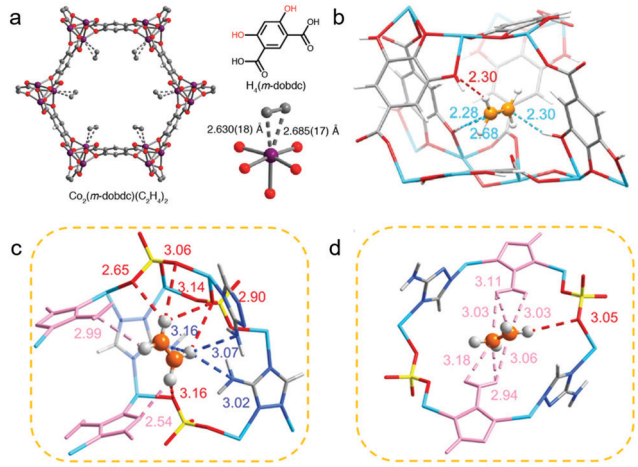

Fig. 12 Illustrations of preferential ethylene binding sites in C_2H_4/C_2H_6 selective adsorbents: (a) **Co_2(*m*-dobdc)**,[99] as determined by *in situ* single-crystal X-ray diffraction under ~0.3 bar of ethylene at 100 K; (b) Mg-gallate, as determined by NPD experiments (the C···H supramolecular interactions of C···H–O and C–D···O H-bonds are marked in cyan and red, respectively);[59] (c and d) $ZnatzPO_4$, as determined by DFT-D calculations.[102] (Reprinted with permissions from ref. 57, 59 and 102: Copyright 2018, Springer Nature; copyright 2018, Wiley-VCH Verlag GmbH & Co. KGaA, Weinheim; copyright, 2020, the authors, some rights reserved; exclusive licensee American Association for the Advancement of Science. Distributed under a Creative Commons Attribution NonCommercial License 4.0 (CC BY-NC) http://creativecommons.org/licenses/by-nc/4.0/.)

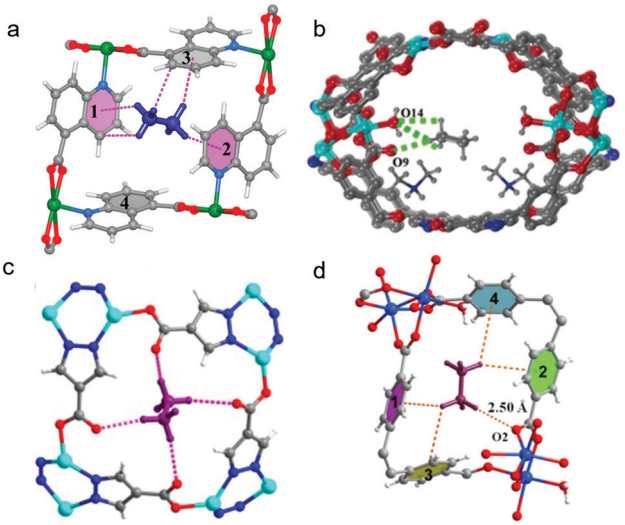

Fig. 13 Preferential ethane binding sites in C_2H_6/C_2H_4 selective adsorbents: (a) Qc-5-Cu-sql-β as determined by NPD experiments;[109] (b) TJT-100, as determined by GCMC simualtions;[70] (c) JNU-2, as determined by DFT-D calculations;[121] (d) NUM-7a, as determined by GCMC simulations.[117] (Reprinted with permissions from ref. 109, 70, 121 and 117; copyright 2018, American Chemical Society; copyright 2018, Wiley-VCH Verlag GmbH & Co. KGaA, Weinheim; copyright 2019, American Chemical Society; copyright 2020, American Chemical Society.)

"molecular trap" like pockets for C_2H_4 (Fig. 12c and d). At site-I (Fig. 12c), C_2H_4 molecules reside close to the pillaring PO_4^{3-} anions and interact with neighbouring O (from PO_4^{3-}) and N atoms (from Atz ligands) *via* weak H-bonds (2.54–3.16 Å) of two types: C–H···O and C–H···N, respectively. C_2H_4 binding site II (Fig. 12d) is centrally placed in the bottleneck-shaped scaffold that connects two adjacent pockets and features weak C–H···O interactions (3.05 Å) between C_2H_4 and the $PO4^{3-}$ pillar. The authors credit the observed equilibrium-kinetic combined C_2H_4/C_2H_6 selectivity of $ZnAtzPO_4$ to the absence of strong H-bonding interactions (C–H···O/N < 2.3 Å) in either of the two aforementioned binding sites. Other examples of C_2H_4 selective physisorbents *versus* C_2H_6 are given in Table 2 and are arranged by decreasing $S_{C_2H_4/C_2H_6}$.

5.6.C. C_2H_6/C_2H_4 separation. Due to increasing kinetic diameter and decreasing quadrupole moment from C_2H_4 to C_2H_6 (Fig. 2), most physisorbents and chemisorbents are selective for C_2H_4 over C_2H_6. C_2H_6/C_2H_4 is therefore considered a "reverse" separation that is of relevance to ethylene purification. Sections 5.2 and 5.4 cover a handful of C_2H_6 capture benchmark materials including MAF-49,[68] $Fe_2(O_2)$(dobdc),[60] and **ZIF-7**.[122,186] Other examples of C_2H_6 selective physisorbents are listed in Table 3 and arranged in order of decreasing $S_{C_2H_6/C_2H_4}$. Three additional examples are now detailed and discussed with respect to the insight they provide from a crystal engineering perspective. It should be noted, however, that no physisorbent has yet exhibited a high enough selectivity to address trace C_2H_6 capture.

A 2D layered PCN studied by us for CO_2 sieving,[192] Qc-5-Cu-sql-β (Qc = quinoline-5-carboxylate), was also studied by B. Chen's group under the name $Cu(Qc)_2$ to examine its $S_{C_2H_6/C_2H_4}$ *vs.* the isostructural isonicotinate variant $Cu(ina)_2$.[109] $Cu(Qc)_2$ exhibits a narrow pore aperture size of 3.3 Å formed by aromatic rings and preferentially adsorbed C_2H_6 over C_2H_4 from calculated IAST selectivity and DCB experiments of an equimolar mixture (1 : 1, v/v). NPD data indicates that C_2H_6 molecules are commensurately packed within the rhombic apertures of $Cu(Qc)_2$ with multiple C–H···π interactions (marked in pink dashed bonds in Fig. 13a).

$(Me_2NH_2)[Co_3(DCPN)_2(\mu_3\text{-}OH)(H_2O)]\cdot 11H_2O$ (DCPN = 5-(3′,5′-dicarboxylphenyl)nicotinate), TJT-100, binds C_2H_2 and C_2H_6 over C_2H_4.[70] Ambient temperature DCB experiments confirmed the potential use of TJT-100 for production of polymer-grade C_2H_4 from a ternary $C_2H_2/C_2H_4/C_2H_6$ (0.5 : 99 : 0.5, v/v/v) mixture. GCMC simulation results suggested that uncoordinated carboxylate oxygen atoms and coordinated water molecules on can trap C_2H_2 and C_2H_6 by formation of multiple C–H···O interactions (Fig. 13b), whereas the corresponding C_2H_4 interaction is much weaker.

The Cu–Zn heterometallic MOF JNU-2 with **xae** topology features cage-like cavities interconnected through 3.7 Å ultramicroporous windows. Its C_2H_6 selectivity as determined by single-component gas sorption isotherms and DCB binary and ternary separation studies (10/90 C_2H_6/C_2H_4, v/v; 10/87/3 $C_2H_6/C_2H_4/C_2H_2$, v/v) was attributed by a molecular modelling study to multiple C–H···O hydrogen bonding interactions at the O-rich pore window. The limiting and cage-connecting pore apertures behaved like screening sites to promote C_2H_6 selectivity, whereas the internal cage porosity enabled high uptake at saturation pressure. C_2H_6 was calculated to form four weak H-bonds with JNU-2 (Fig. 13c) *vs.* only two H-bonds for C_2H_4. The DFT-D modelled observation on binding energy difference

of 6.2 kJ mol^{-1} is consistent with that in electrostatic interactions (7.7 kJ mol^{-1}) attributable to two weak H-bonds.

T.-L. Hu's group prepared the 3D ultramicroporous MOF NUM-7a by activating as-synthesised $[Mn_2(TCPE)(DMF)(H_2O)]\cdot DMF\cdot CH_3CN$ (TCPE = 4,4′,4″,4‴-(ethene-1,1,2,2-tetrayl)tetrabenzoate).[117] The narrow pore aperture of 3.42 Å facilitated C–H···O and C–H···π interactions (Fig. 13d) upon adsorption of C_2H_6. NUM-7a is another PCN that exhibits a "best fit" for C_2H_6 *vs.* the other C2 LHs. Planar configurations of adsorbed C_2H_2 and C_2H_4 restrict their weak interactions with the surrounding benzoate O-atoms and phenyl rings, as discussed therein.

5.6.D. C_2H_2/CO_2 and CO_2/C_2H_2 separation. As noted above in Section 4 and Fig. 4, one of the earliest reports of C2 separation was from Kitagawa's group in 2005. CPL-1[62] introduced a binding site concept to explain C_2H_2/CO_2 selectivity and potential separation. This report was followed shortly thereafter by the study of $M(HCOO)_2$ (M = Mg and Mn) (Fig. 4).[69] Since these initial reports on PCNs, the number of C_2H_2/CO_2 and CO_2/C_2H_2 selective adsorbents that have been reported is relatively low, presumably because of the identical kinetic diameters, close quadrupole moments and proximal boiling points of the two gases (Fig. 2). In essence, these physicochemical properties practically rule out molecular sieving and require other mechanisms (Fig. 5) for effective separation(s). In Sections 5.2 and 5.4, we detailed two C_2H_2 binding sites that stand out as examples of C_2H_2/CO_2 selective PCNs (UTSA-300a[52] and TCuCl:[64] Fig. 9b and 7d, respectively), whereas CO_2/C_2H_2 separation was effected by the PCN Mn(bdc)(dpe)[164] (Fig. 9c). We now detail three examples of selective binding sites: **SIFSIX-3-Ni**[47] for CO_2/C_2H_2 selectivity; $[Ni_3(HCOO)_6]$,[133] and ZJU-74a[53] for C_2H_2/CO_2 selective PCNs.

Selectivity for CO_2 *vs.* C_2H_2 has only been reported for six physisorbents, five of them being PCNs (Table 4). Apart from [Mn(bdc)(dpe)][164] and the thulium(III) nitrate based material Tm(OH-bdc)[162] (OH-bdc = 2,5-dihydroxyterephthalate), **SIFSIX-3-Ni** is the only example of a physisorbent that has been reported to exhibit CO_2/C_2H_2 separation under DCB experimental conditions.[47] GCMC simulations conducted upon **SIFSIX-3-Ni** suggested that, upon full saturation, C_2H_2 molecules align in a slipped parallel orientation to commensurately pack with two molecules per unit cell (Fig. 14a, left). Each C_2H_2 orients in a manner that allows C–H···C–H sorbate–sorbate interactions on both sides and a favourable C–H···F interaction on one side. In contrast, the single binding site for CO_2 in **SIFSIX-3-Ni** was calculated and experimentally validated in an earlier *in situ* study.[193] CO_2 molecules are proximate to the four electro-negative F atoms from four independent SiF_6^{2-} pillars with $C^{\delta+}\cdots F^{\delta-}$ contacts of ~2.75 Å (Fig. 14a, right). A 10 : 5 : 85 C_2H_2 : CO_2 : He DCB experiment validated CO_2/C_2H_2 binary separation that produces high-purity C_2H_2 effluent in a one-step adsorption process that does not need an energy-intensive regeneration step.

Early reports with metal formates[69] prompted B. Chen and Qian's groups to explore the moisture and H_2S-stable MOF $[Ni_3(HCOO)_6]_n$ for C_2H_2/CO_2 equimolar (v/v) separation.[133] The ultramicroporous aperture of 4.3 Å and O donor sites from formate ligands on the pore walls enable moderate selectivity for C_2H_2 as validated by GCMC simulations which revealed that each unit cell binds one C_2H_2 molecule through such H-bonding (Fig. 14b).

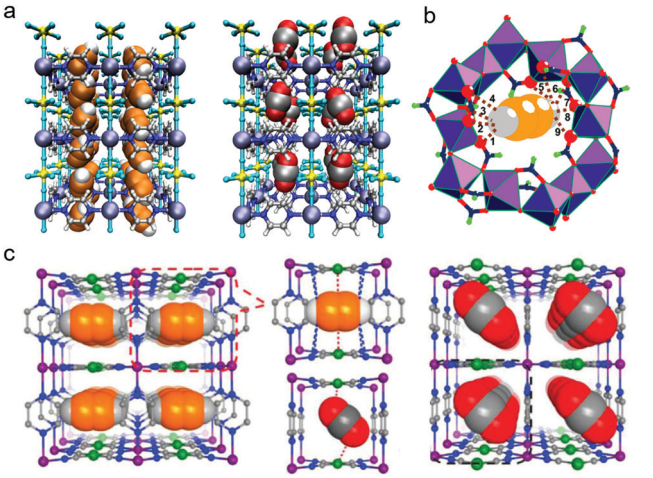

Fig. 14 Illustrations of preferential binding sites for (a) C_2H_2 (left) and CO_2 (right) in **SIFSIX-3-Ni** as determined by GCMC simulations;[47] (b) C_2H_2 in $[Ni_3(HCOO)_6]$, as determined by GCMC simulations;[133] (c) C_2H_2 and CO_2 in ZJU-74a as determined by GCMC simulations.[53] (Reprinted with permissions from ref. 47, 133 and 53; copyright 2016, Elsevier Inc.; copyright 2019, American Chemical Society; copyright 2020, Wiley-VCH Verlag GmbH & Co. KGaA, Weinheim.)

Ultramicroporous pillared Hofmann clathrate sorbents are a promising but understudied PCN platform for adsorptive separation studies. Recent reports suggested their possible utility for selective C_2H_2 adsorption.[53,54] In ZJU-74a, reported by Qian and coworkers in 2020, a "sandwich-type" binding site is created by the exposed square planar Ni(II) centres located 3.6 Å apart at diametrically opposite positions in a cuboidal pore. GCMC simulations revealed that the Ni(II) centres interact strongly with the C≡C bond of acetylene, while eight C≡N N atoms from two different $[Ni(CN)_4]^{2-}$ groups are H-bonded to the H atoms of C_2H_2, creating a tight, specific binding site (Fig. 14c). The effect of this cooperative "sandwich-type" binding site can be seen in the very high IAST selectivity of ZJU-74a for C_2H_2/CO_2 separation (36.5), which in turn results in excellent DCB separation performance with dry and wet equimolar C_2H_2/CO_2 mixtures. A high selectivity for C_2H_2 over C_2H_4 was also reported and 1 : 99 C_2H_2/C_2H_4 DCB experiments demonstrated trace acetylene removal. The chemical stability of ZJU-74a is an advantage for development at higher technological readiness levels (TRLs).[53]

5.7. Separation of multi-component gas mixtures by SSST

Whereas we and others have tended to focus upon binary separations, the most relevant industrial gas mixtures (*e.g.* biogas, syngas, air, natural gas, C2 gases, C3 gases) are multi-component gas mixtures of varying composition. As detailed herein, advances in the past five years have provided families of physisorbents that exhibit new selectivity benchmarks for each of the trace impurities present in the most relevant gas

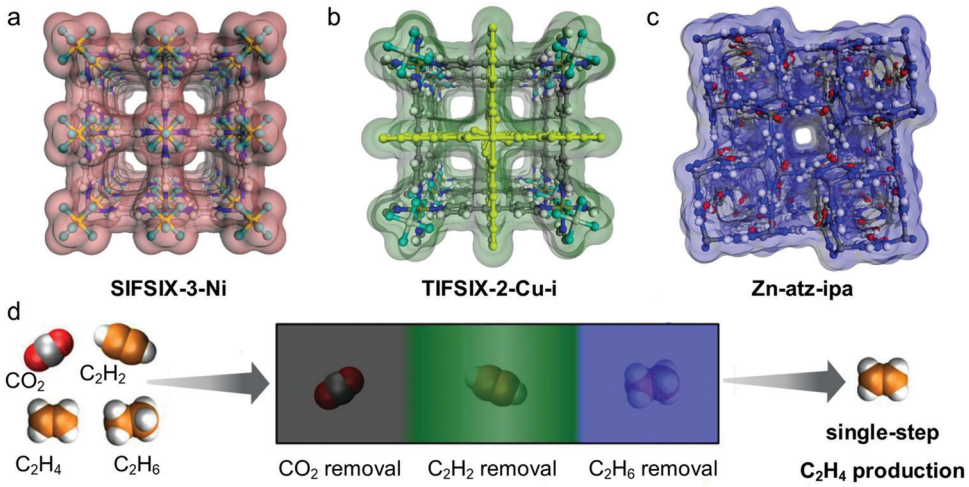

Fig. 15 (a–c) 1D ultramicroporous channels in the **pcu** topology PCN sorbents (a) **SIFSIX-3-Ni**, (b) **TIFSIX-2-Cu-i** and (c) **Zn-atz-ipa**, respectively; (d) SSST to purify C_2H_4 in one-step from a $CO_2/C_2H_2/C_2H_4/C_2H_6$ quaternary gas mixture.

mixtures.[38,40–42,64,68,76] To address purification of the largest volume chemical building block chemical, C_2H_4, we recently introduced the use of multiple bespoke sorbents to enable "synergistic sorbent separation technology", SSST, for the one-step production of polymer-grade (>99.9% purity) C_2H_4 from ternary ($C_2H_2/C_2H_6/C_2H_4$) or quaternary ($CO_2/C_2H_2/C_2H_6/C_2H_4$) gas mixtures. SSST was demonstrated with a column packed with a series of three ultramicroporous PCNs, **SIFSIX-3-Ni**,[194] **TIFSIX-2-Cu-i**[47] and **Zn-atz-ipa**,[195] in a packed-bed geometry (Fig. 15).[71] SSST exploited the three bespoke physisorbents, one for each trace impurity, to enable single-step removal of multiple impurities. This approach enabled one-step purification of multicomponent gas mixtures that mimic real-world gas mixtures. That SSST was effective under two different quaternary mixture concentrations: 1:33:33:33 and 1:1:1:1, implies that the choice of task-specific ultraselective sorbents in tandem-packed sorbent beds of the type used here is unlikely to be limited to the three sorbents or gas mixtures that we investigated. Further, performance could be enhanced by substitution of second generation sorbents with higher selectivity, higher uptake capacity, or both, to optimize overall performance. The strong performance of SSST with respect to the purification of C2 gas mixtures and the availability of an ever-increasing number of ultraselective physisorbents suggests that the scope of SSST will be broad enough to address the high energy footprint of other industrial commodity purifications.

6. Critical analysis and future outlook

Herein, we have detailed the emergence and rapid development of PCNs as physisorbents for the challenging and industrially important separation of C2 LHs. We have also delineated structure–function relationships in terms of pore structure, size and chemistry and how they impact sorbent–sorbate interactions at the molecular level. PCNs have thereby emerged as the leading adsorbent class for C2 separations to the extent that they now represent a greater share of research output in this area than all other classes of sorbents combined (Fig. 3). We attribute this upsurge of interest to the exceptional tunability of pore size and pore chemistry offered by PCNs that has enabled unmatched selectivities for C2 separations through careful control of pore dimensions (to exclude larger adsorbates) or the incorporation of bespoke functionalities to enhance sorbate binding. Crystal engineering of PCN adsorbents has thereby enabled the design of new generations of sorbents with favourable thermodynamics for selective binding, energy-efficient regeneration (Q_{st} ~ 35–50 kJ mol^{-1}) and fast sorption kinetics.[6,45] These characteristics are perhaps best exemplified by ultramicroporous (<0.7 nm) PCNs as pioneered by several groups, including ours. The combination of strongly interacting functional groups (*e.g.* inorganic anions) and narrow channels results in tight fitting binding sites that offer highly specific interactions for key adsorbates. This is borne out by a comparison of the leading physisorbents for the binary C2 separations detailed herein. Plots of IAST selectivity *versus* uptake (Fig. 16) reveal that several ultramicroporous PCNs are the best performing class of materials, sometimes orders of magnitude ahead of their larger-pore counterparts. Indeed, the top performing materials for C_2H_2/C_2H_4, C_2H_4/C_2H_6 and C_2H_2/CO_2 selectivity are all ultramicroporous PCNs.

We also note that the ultramicroporous sorbents with tight binding sites have resulted in examples of 'reverse selectivity' such as C_2H_6/C_2H_4 and CO_2/C_2H_2 selective sorbents. These sorbents are not outliers. Rather, they are powerful illustrations of how pore structure, chemistry and shape can lead to profound property effects and task-specific binding sites. Whereas crystal engineering of binding sites with just the right charge distributions to harness the slight differences in hard-to-separate sorbate pairs remains challenging, growing insight into the mechanisms underlying this type of 'reverse' selectivity, have been aided by computational chemistry and *in situ* structural studies. Even when adsorbates are of the same kinetic diameter (or indeed, the larger one is selectively adsorbed), ultramicroporous PCNs

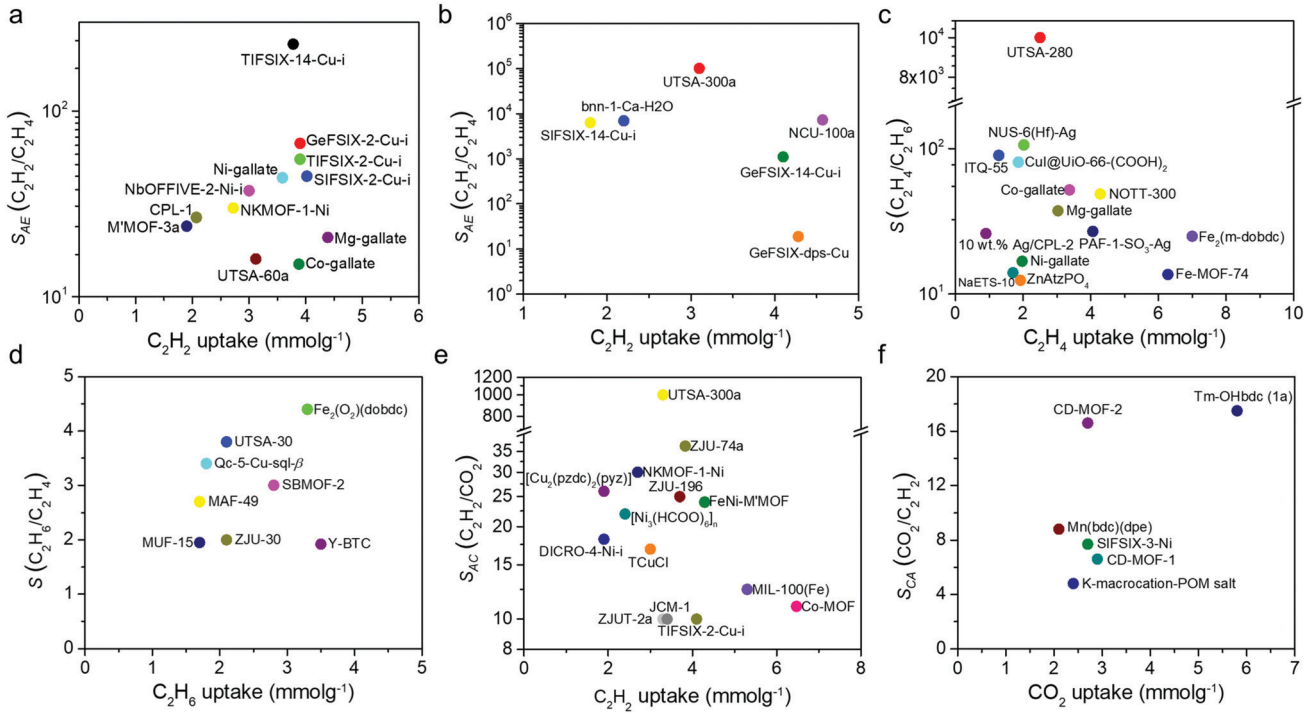

Fig. 16 Selectivity *versus* uptake plots for (a) C_2H_2/C_2H_4 selective adsorbents with a threshold C_2H_2 selectivity, $S_{AE} > 15$ (calculated for 1 : 99 mixtures of $C_2H_2 : C_2H_4$ unless otherwise stated in Table 1); (b) C_2H_2/C_2H_4 selective adsorbents that exhibit molecular sieving (calculated for 1 : 99 mixtures of $C_2H_2 : C_2H_4$ unless otherwise stated in Table 1). The IAST derived selectivities are therefore qualitative; (c) C_2H_4/C_2H_6 selective adsorbents with a threshold C_2H_4 selectivity, $S_{C_2H_4/C_2H_6} > 10$ (calculated for 1 : 1 mixtures of $C_2H_4 : C_2H_6$,unless otherwise stated in Table 2); (d) C_2H_6/C_2H_4 selective adsorbents with a threshold C_2H_6 selectivity, $S_{C_2H_6/C_2H_4} > 1.9$ (calculated for 1 : 1 mixtures of $C_2H_6 : C_2H_4$ unless otherwise stated in Table 3); (e) C_2H_2/CO_2 selective adsorbents with a threshold C_2H_2 selectivity, $S_{AC} > 10$ (calculated for 1 : 1 mixtures of $C_2H_2 : CO_2$ unless otherwise stated in Table 4); (f) CO_2/C_2H_2 selective adsorbents (calculated for 1 : 1 or 2 : 1 mixtures of $CO_2 : C_2H_2$ as stated in Table 4). Uptakes and selectivities are considered at 1 bar, at the temperatures specified in Tables 1–4.

feature among the top performing adsorbents and demonstrate their versatility as tunable sorbent platforms.[28]

The body of research on C2 LHs has established that crystal engineering can take first generation PCNs with benchmark properties and quickly iterate families of second generation PCNs with even better C2 separation performance. Nevertheless, in order for PCNs to replace existing separation technologies, some obstacles must be overcome. Future research must address the full "*spectrum of performance parameters*" that is relevant to commercial applications (Fig. 17). Since the eventual goal of the development of sorbents is industrial utility, factors such as cost, stability, scale-up and multi-cycle regenerability must also be considered, beginning at the lab scale.

In addition, the study of highly selective flexible adsorbents is in its infancy and is still looking at first generation materials for which the thermodynamics and kinetics of phase transformations remain poorly understood. Nevertheless, the high working capacities that can arise from type F-IV isotherms could lead to benchmark separation performance. In this context, whether selectivity is retained in the 'open' phase also remains understudied. Advanced *in situ* techniques[196] that provide clues to the processes underlying stimulus-responsive adsorption[197] are needed for further development of flexible C2-selective adsorbents.

Several other aspects of PCN sorbent performance remain understudied. For example, adsorption/desorption kinetics and co-adsorption are areas that must be addressed. In addition, multicomponent dynamic column breakthrough experiments can provide vital insight into the performance of sorbents under industrially relevant conditions with more complex gas

Fig. 17 The spectrum of performance parameters that must be exhibited by a sorbent with respect to gas separation/purification technologies.

mixtures than those typically studied at the lab scale. The stability of candidate PCNs to H_2, CO and sulphur-containing compounds, as well as the retention of their performance is also an important factor in determining the viability of sorbents at higher TRLs.[198,199] The further development of 'reverse' selectivity in, for example, C_2H_6/C_2H_4 and CO_2/C_2H_2 separations, is also an area for that needs more study and insight. Reverse selectivity can be advantageous for removal of common trace impurities from feedstock gases during the adsorption cycle of fixed-bed processes. Synergistic sorbent separation technology, as put forward by our group, is a recent highlight in this context.[71] The use of combinations of two or more sorbents with specific properties offers an simple but effective approach to the challenge of multicomponent ''*real-world*'' gas mixtures of varying composition.

In summary, crystal engineering of PCN platforms has enabled fine tuning of families of ultramicroporous PCNs that offer new benchmarks for separation performances of C2 LHs, but in many ways we are only at the end of the beginning. Moving forward, the next steps will involve the design and discovery of third generation sorbents that offer strong separation performances addressing other properties that collectively enable further development of PCN sorbents at higher TRLs.

Conflicts of interest

The authors have no conflicts of interest to declare.

Acknowledgements

The authors acknowledge the generous support of Science Foundation Ireland (13/RP/B2549 and 16/IA/4624). S. M. thanks the Alexander von Humboldt Foundation for awarding a post-doctoral research fellowship and Prof. Dr Roland A. Fischer (Chair of Inorganic and Metal–Organic Chemistry, TU Munich) for hosting his research tenure.

Notes and references

1 https://www.icca-chem.org/wp-content/uploads/2019/03/ICCA_EconomicAnalysis_Report_030819.pdf, Report for International Council of Chemical Associations (ICCA), accessed 04/07/2020.
2 S. Kitagawa, *Angew. Chem., Int. Ed.*, 2015, **54**, 10686–10687.
3 D. S. Sholl and R. P. Lively, *Nature*, 2016, **532**, 435–437.
4 Z. Bao, G. Chang, H. Xing, R. Krishna, Q. Ren and B. Chen, *Energy Environ. Sci.*, 2016, **9**, 3612–3641.
5 D. G. Madden, D. O'Nolan, K.-J. Chen, C. Hua, A. Kumar, T. Pham, K. A. Forrest, B. Space, J. J. Perry and M. Khraisheh, *Chem. Commun.*, 2019, **55**, 3219–3222.
6 W.-G. Cui, T.-L. Hu and X.-H. Bu, *Adv. Mater.*, 2020, **32**, 1806445.
7 T. Ren, M. K. Patel and K. Blok, *Energy*, 2008, **33**, 817–833.
8 https://cefic.org/app/uploads/2019/01/The-European-Chemical-Industry-Facts-And-Figures-2020.pdf, Conseil Européen des Fédérations de l'Industrie Chimique, accessed 04/07/2020.
9 L. Meng, L. Yang, C. Chen, X. Dong, S. Ren, G. Li, Y. Li, Y. Han, Z. Shi and S. Feng, *ACS Appl. Mater. Interfaces*, 2020, **12**, 5999–6006.
10 Y. Wang, S. B. Peh and D. Zhao, *Small*, 2019, **15**, 1900058.
11 L. Kniel, O. Winter and K. Stork, *Ethylene: Keystone to the petrochemical industry*, Dekker, 1980.
12 J. J. McKetta Jr, *Encyclopedia of Chemical Processing and Design: Volume 20 - Ethanol as Fuel*, CRC Press, 1984.
13 J. H. Kang, E. W. Shin, W. J. Kim, J. D. Park and S. H. Moon, *Catal. Today*, 2000, **63**, 183–188.
14 S. Sircar, *Ind. Eng. Chem. Res.*, 2006, **45**, 5435–5448.
15 J.-R. Li, R. J. Kuppler and H.-C. Zhou, *Chem. Soc. Rev.*, 2009, **38**, 1477–1504.
16 D. R. Lide, *CRC handbook of chemistry and physics*, CRC Press, 2004.
17 M. Neelis, M. Patel, K. Blok, W. Haije and P. Bach, *Energy*, 2007, **32**, 1104–1123.
18 P. Pässler, W. Hefner, K. Bucki, H. Meinass, A. Meiswinkel, H. Wernicke, G. Ebersberg, R. Muller, J. Bässler and H. Behringer, Acetylene, *Ullmann's Encyclopedia of Industrial Chemistry*, 2011, DOI: 10.1002/14356007.a01_097.pub4.
19 K. Weissermel, H.-J. Arpe, C. R. Lindley and S. Hawkins, *Industrial organic chemistry*, Wiley Online Library, 1997.
20 H. Schobert, *Chem. Rev.*, 2014, **114**, 1743–1760.
21 S. H. Pine, J. Hendrickson, D. Cram and G. Hammond, *Organic Chemistry*, McGraw-Hill Book Company, New York City, 1987.
22 R. E. Gannon, V. J. Krukonis and T. Schoenberg, *Product R&D*, 1970, **9**, 343–347.
23 Ascent Supply Chain Consultants Pvt. Ltd Calcium Carbide, https://www.ascconline.com/img/services/project_report/Calcium_Carbide_Project_Report_Sample.pdf, (accessed 04/07/2020).
24 N. Magnowski, A. Avila, C. Lin, M. Shi and S. Kuznicki, *Chem. Eng. Sci.*, 2011, **66**, 1697–1701.
25 S. Matar and L. F. Hatch, *Chemistry of petrochemical processes*, Elsevier, 2001.
26 S. Bhattacharya, K. S. Peraka and M. J. Zaworotko, *Co-crystals: Preparation, Characterization and Applications*, The Royal Society of Chemistry, 2018, pp. 33–79, DOI: 10.1039/9781788012874-00033.
27 S. Ma and H.-C. Zhou, *J. Am. Chem. Soc.*, 2006, **128**, 11734–11735.
28 S. Mukherjee and M. J. Zaworotko, *Trends Chem.*, 2020, **2**, 506–518.
29 B. Moulton and M. J. Zaworotko, *Chem. Rev.*, 2001, **101**, 1629–1658.
30 B. F. Hoskins and R. Robson, *J. Am. Chem. Soc.*, 1990, **112**, 1546–1554.
31 S. R. Batten, N. R. Champness, X.-M. Chen, J. Garcia-Martinez, S. Kitagawa, L. Öhrström, M. O'Keeffe, M. Paik Suh and J. Reedijk, *Pure Appl. Chem.*, 2013, **85**, 1715.
32 M. Kondo, T. Yoshitomi, H. Matsuzaka, S. Kitagawa and K. Seki, *Angew. Chem., Int. Ed. Engl.*, 1997, **36**, 1725–1727.
33 H. Li, M. Eddaoudi, T. L. Groy and O. M. Yaghi, *J. Am. Chem. Soc.*, 1998, **120**, 8571–8572.
34 S. S. Y. Chui, S. M. F. Lo, J. P. H. Charmant, A. G. Orpen and I. D. Williams, *Science*, 1999, **283**, 1148.
35 H. Li, M. Eddaoudi, M. O'Keeffe and O. M. Yaghi, *Nature*, 1999, **402**, 276–279.
36 I. M. Hönicke, I. Senkovska, V. Bon, I. A. Baburin, N. Bönisch, S. Raschke, J. D. Evans and S. Kaskel, *Angew. Chem., Int. Ed.*, 2018, **57**, 13780–13783.
37 O. K. Farha, I. Eryazici, N. C. Jeong, B. G. Hauser, C. E. Wilmer, A. A. Sarjeant, R. Q. Snurr, S. T. Nguyen, A. Ö. Yazaydın and J. T. Hupp, *J. Am. Chem. Soc.*, 2012, **134**, 15016–15021.
38 P. Nugent, Y. Belmabkhout, S. D. Burd, A. J. Cairns, R. Luebke, K. Forrest, T. Pham, S. Ma, B. Space, L. Wojtas, M. Eddaoudi and M. J. Zaworotko, *Nature*, 2013, **495**, 80–84.
39 P. M. Bhatt, Y. Belmabkhout, A. Cadiau, K. Adil, O. Shekhah, A. Shkurenko, L. J. Barbour and M. Eddaoudi, *J. Am. Chem. Soc.*, 2016, **138**, 9301–9307.
40 S. Mukherjee, N. Sikdar, D. O'Nolan, D. M. Franz, V. Gascón, A. Kumar, N. Kumar, H. S. Scott, D. G. Madden and P. E. Kruger, *Sci. Adv.*, 2019, **5**, eaax9171.
41 X. Cui, K. Chen, H. Xing, Q. Yang, R. Krishna, Z. Bao, H. Wu, W. Zhou, X. Dong, Y. Han, B. Li, Q. Ren, M. J. Zaworotko and B. Chen, *Science*, 2016, **353**, 141–144.
42 B. Li, X. Cui, D. O'Nolan, H.-M. Wen, M. Jiang, R. Krishna, H. Wu, R.-B. Lin, Y.-S. Chen, D. Yuan, H. Xing, W. Zhou, Q. Ren, G. Qian, M. J. Zaworotko and B. Chen, *Adv. Mater.*, 2017, **29**, 1704210.
43 D. O'Nolan, A. Kumar and M. J. Zaworotko, *J. Am. Chem. Soc.*, 2017, **139**, 8508–8513.
44 X. Liu, X. Wang and F. Kapteijn, *Chem. Rev.*, 2020, DOI: 10.1021/acs.chemrev.9b00746.
45 R.-B. Lin, S. Xiang, W. Zhou and B. Chen, *Chem*, 2020, **6**, 337–363.
46 B. Chen, M. Eddaoudi, S. T. Hyde, M. O'Keeffe and O. M. Yaghi, *Science*, 2001, **291**, 1021–1023.
47 K.-J. Chen, H. S. Scott, D. G. Madden, T. Pham, A. Kumar, A. Bajpai, M. Lusi, K. A. Forrest, B. Space, J. J. Perry and M. J. Zaworotko, *Chem*, 2016, **1**, 753–765.

48 H. Nonnenmacher *et al.*, Production of acetylene by thermal cracking of liquid hydrocarbons, *US Pat.*, US3242223A, 1966.
49 S. Mukherjee, Y. He, D. Franz, S.-Q. Wang, W.-R. Xian, A. Bezrukov, B. Space, Z. Xu, J. He and M. Zaworotko, *Chem. – Eur. J.*, 2020, **26**, 4923–4929.
50 R. Chebbi, N. Al-Amoodi, N. A. Jabbar, G. Husseini and K. Al Mazroui, *Chem. Eng. Res. Des.*, 2010, **88**, 779–787.
51 S. Brueske, C. Kramer and A. Fisher, *Bandwidth Study on Energy Use and Potential Energy Saving Opportunities in US Chemical Manufacturing*, Energetics, 2015.
52 R.-B. Lin, L. Li, H. Wu, H. Arman, B. Li, R.-G. Lin, W. Zhou and B. Chen, *J. Am. Chem. Soc.*, 2017, **139**, 8022–8028.
53 J. Pei, K. Shao, J.-X. Wang, H.-M. Wen, Y. Yang, Y. Cui, R. Krishna, B. Li and G. Qian, *Adv. Mater.*, 2020, **32**, 1908275.
54 J. Gao, X. Qian, R.-B. Lin, R. Krishna, H. Wu, W. Zhou and B. Chen, *Angew. Chem., Int. Ed.*, 2020, **59**, 4396–4400.
55 J. Wang, Y. Zhang, P. Zhang, J. Hu, R.-B. Lin, Q. Deng, Z. Zeng, H. Xing, S. Deng and B. Chen, *J. Am. Chem. Soc.*, 2020, **142**, 9744–9751.
56 S. Mukherjee, S. Chen, A. Bezrukov, M. Mostrom, V. Terskikh, D. Franz, S.-Q. Wang, A. Kumar, M. Chen, B. Space, Y. Huang and M. J. Zaworotko, *Angew. Chem., Int. Ed.*, 2020, DOI: 10.1002/anie.202006414.
57 R.-B. Lin, L. Li, H.-L. Zhou, H. Wu, C. He, S. Li, R. Krishna, J. Li, W. Zhou and B. Chen, *Nat. Mater.*, 2018, **17**, 1128–1133.
58 L. Zhang, L. Li, E. Hu, L. Yang, K. Shao, L. Yao, K. Jiang, Y. Cui, Y. Yang, B. Li, B. Chen and G. Qian, *Adv. Sci.*, 2020, **7**, 1901918.
59 Z. Bao, J. Wang, Z. Zhang, H. Xing, Q. Yang, Y. Yang, H. Wu, R. Krishna, W. Zhou, B. Chen and Q. Ren, *Angew. Chem., Int. Ed.*, 2018, **57**, 16020–16025.
60 L. Li, R.-B. Lin, R. Krishna, H. Li, S. Xiang, H. Wu, J. Li, W. Zhou and B. Chen, *Science*, 2018, **362**, 443–446.
61 Y. He, S. Xiang, Z. Zhang, S. Xiong, F. R. Fronczek, R. Krishna, M. O'Keeffe and B. Chen, *Chem. Commun.*, 2012, **48**, 10856–10858.
62 R. Matsuda, R. Kitaura, S. Kitagawa, Y. Kubota, R. V. Belosludov, T. C. Kobayashi, H. Sakamoto, T. Chiba, M. Takata, Y. Kawazoe and Y. Mita, *Nature*, 2005, **436**, 238–241.
63 H.-M. Wen, C. Liao, L. Li, L. Yang, J. Wang, L. Huang, B. Li, B. Chen and J. Hu, *Chem. Commun.*, 2019, **55**, 11354–11357.
64 S. Mukherjee, Y. He, D. Franz, S.-Q. Wang, W.-R. Xian, A. A. Bezrukov, B. Space, Z. Xu, J. He and M. J. Zaworotko, *Chem. – Eur. J.*, 2020, **26**, 4923–4929.
65 S.-C. Xiang, Z. Zhang, C.-G. Zhao, K. Hong, X. Zhao, D.-R. Ding, M.-H. Xie, C.-D. Wu, M. C. Das, R. Gill, K. M. Thomas and B. Chen, *Nat. Commun.*, 2011, **2**, 204.
66 E. D. Bloch, W. L. Queen, R. Krishna, J. M. Zadrozny, C. M. Brown and J. R. Long, *Science*, 2012, **335**, 1606–1610.
67 S. Yang, A. J. Ramirez-Cuesta, R. Newby, V. Garcia-Sakai, P. Manuel, S. K. Callear, S. I. Campbell, C. C. Tang and M. Schröder, *Nat. Chem.*, 2015, **7**, 121–129.
68 P.-Q. Liao, W.-X. Zhang, J.-P. Zhang and X.-M. Chen, *Nat. Commun.*, 2015, **6**, 8697.
69 D. G. Samsonenko, H. Kim, Y. Sun, G.-H. Kim, H.-S. Lee and K. Kim, *Chem. – Asian J.*, 2007, **2**, 484–488.
70 H.-G. Hao, Y.-F. Zhao, D.-M. Chen, J.-M. Yu, K. Tan, S. Ma, Y. Chabal, Z.-M. Zhang, J.-M. Dou, Z.-H. Xiao, G. Day, H.-C. Zhou and T.-B. Lu, *Angew. Chem., Int. Ed.*, 2018, **57**, 16067–16071.
71 K.-J. Chen, D. G. Madden, S. Mukherjee, T. Pham, K. A. Forrest, A. Kumar, B. Space, J. Kong, Q.-Y. Zhang and M. J. Zaworotko, *Science*, 2019, **366**, 241–246.
72 D. O'Nolan, A. Kumar, K.-J. Chen, S. Mukherjee, D. G. Madden and M. J. Zaworotko, *ACS Appl. Nano Mater.*, 2018, **1**, 6000–6004.
73 Z. Zhang, X. Cui, L. Yang, J. Cui, Z. Bao, Q. Yang and H. Xing, *Ind. Eng. Chem. Res.*, 2018, **57**, 7266–7274.
74 J. Wang, L. Li, L. Guo, Y. Zhao, D. Xie, Z. Zhang, Q. Yang, Y. Yang, Z. Bao and Q. Ren, *Chem. – Eur. J.*, 2019, **25**, 15516–15524.
75 L. Yang, A. Jin, L. Ge, X. Cui and H. Xing, *Chem. Commun.*, 2019, **55**, 5001–5004.
76 Y. L. Peng, T. Pham, P. Li, T. Wang, Y. Chen, K. J. Chen, K. A. Forrest, B. Space, P. Cheng and M. J. Zaworotko, *Angew. Chem., Int. Ed.*, 2018, **57**, 10971–10975.
77 F. Zheng, L. Guo, B. Gao, L. Li, Z. Zhang, Q. Yang, Y. Yang, B. Su, Q. Ren and Z. Bao, *ACS Appl. Mater. Interfaces*, 2019, **11**, 28197–28204.
78 H.-M. Wen, B. Li, H. Wang, C. Wu, K. Alfooty, R. Krishna and B. Chen, *Chem. Commun.*, 2015, **51**, 5610–5613.
79 L. Li, R.-B. Lin, R. Krishna, X. Wang, B. Li, H. Wu, J. Li, W. Zhou and B. Chen, *J. Mater. Chem. A*, 2017, **5**, 18984–18988.
80 G.-X. Jin, X. Niu, J. Wang, J.-P. Ma, T.-L. Hu and Y.-B. Dong, *Chem. Mater.*, 2018, **30**, 7433–7437.
81 D.-M. Chen, C.-X. Sun, N.-N. Zhang, H.-H. Si, C.-S. Liu and M. Du, *Inorg. Chem.*, 2018, **57**, 2883–2889.
82 T.-L. Hu, H. Wang, B. Li, R. Krishna, H. Wu, W. Zhou, Y. Zhao, Y. Han, X. Wang, W. Zhu, Z. Yao, S. Xiang and B. Chen, *Nat. Commun.*, 2015, **6**, 7328.
83 H. Li, L. Li, R.-B. Lin, G. Ramirez, W. Zhou, R. Krishna, Z. Zhang, S. Xiang and B. Chen, *ACS Sustainable Chem. Eng.*, 2019, **7**, 4897–4902.
84 O. T. Qazvini, R. Babarao and S. G. Telfer, *Chem. Mater.*, 2019, **31**, 4919–4926.
85 J. Lee, C. Y. Chuah, J. Kim, Y. Kim, N. Ko, Y. Seo, K. Kim, T. H. Bae and E. Lee, *Angew. Chem., Int. Ed.*, 2018, **57**, 7869–7873.
86 J. Xiong, A. Li, Y. Fan, Z. Xu, H. Feng, Q. Gao, Q. Fan, Y. He, Z. Gao and F. Luo, *J. Solid State Chem.*, 2020, **288**, 121337.
87 L. Zhang, X. Cui, H. Xing, Y. Yang, Y. Cui, B. Chen and G. Qian, *RSC Adv.*, 2017, **7**, 20795–20800.
88 H.-M. Wen, B. Li, H. Wang, R. Krishna and B. Chen, *Chem. Commun.*, 2016, **52**, 1166–1169.
89 J. Li, L. Jiang, S. Chen, A. Kirchon, B. Li, Y. Li and H.-C. Zhou, *J. Am. Chem. Soc.*, 2019, **141**, 3807–3811.
90 H.-H. Wang, Q.-Y. Liu, L. Li, R. Krishna, Y.-L. Wang, X.-W. Peng, C.-T. He, R.-B. Lin and B. Chen, *Inorg. Chem.*, 2018, **57**, 9489–9494.
91 F. Yu, B.-Q. Hu, X.-N. Wang, Y.-M. Zhao, J.-L. Li, B. Li and H.-C. Zhou, *J. Mater. Chem. A*, 2020, **8**, 2083–2089.
92 Y. He, R. Krishna and B. Chen, *Energy Environ. Sci.*, 2012, **5**, 9107–9120.
93 X. Wang, L. Li, Y. Wang, J.-R. Li and J. Li, *CrystEngComm*, 2017, **19**, 1729–1737.
94 T. Ke, Q. Wang, J. Shen, J. Zhou, Z. Bao, Q. Yang and Q. Ren, *Angew. Chem., Int. Ed.*, 2020, **59**, 12725–12730.
95 Y. Wang, Z. Hu, Y. Cheng and D. Zhao, *Ind. Eng. Chem. Res.*, 2017, **56**, 4508–4516.
96 P. J. Bereciartua, Á. Cantín, A. Corma, J. L. Jordá, M. Palomino, F. Rey, S. Valencia, E. W. Corcoran, P. Kortunov, P. I. Ravikovitch, A. Burton, C. Yoon, Y. Wang, C. Paur, J. Guzman, A. R. Bishop and G. L. Casty, *Science*, 2017, **358**, 1068–1071.
97 B. Li, Y. Zhang, R. Krishna, K. Yao, Y. Han, Z. Wu, D. Ma, Z. Shi, T. Pham, B. Space, J. Liu, P. K. Thallapally, J. Liu, M. Chrzanowski and S. Ma, *J. Am. Chem. Soc.*, 2014, **136**, 8654–8660.
98 H. Xiang, A. Ameen, J. Shang, Y. Jiao, P. Gorgojo, F. R. Siperstein and X. Fan, *Microporous Mesoporous Mater.*, 2020, **293**, 109784.
99 J. E. Bachman, M. T. Kapelewski, D. A. Reed, M. I. Gonzalez and J. R. Long, *J. Am. Chem. Soc.*, 2017, **139**, 15363–15370.
100 A. Anson, Y. Wang, C. C. H. Lin, T. M. Kuznicki and S. M. Kuznicki, *Chem. Eng. Sci.*, 2008, **63**, 4171–4175.
101 R. Vaidhyanathan, S. S. Iremonger, G. K. H. Shimizu, P. G. Boyd, S. Alavi and T. K. Woo, *Angew. Chem., Int. Ed.*, 2012, **51**, 1826–1829.
102 Q. Ding, Z. Zhang, C. Yu, P. Zhang, J. Wang, X. Cui, C.-H. He, S. Deng and H. Xing, *Sci. Adv.*, 2020, **6**, eaaz4322.
103 Y. Zhang, B. Li, R. Krishna, Z. Wu, D. Ma, Z. Shi, T. Pham, K. Forrest, B. Space and S. Ma, *Chem. Commun.*, 2015, **51**, 2714–2717.
104 G. Chang, M. Huang, Y. Su, H. Xing, B. Su, Z. Zhang, Q. Yang, Y. Yang, Q. Ren, Z. Bao and B. Chen, *Chem. Commun.*, 2015, **51**, 2859–2862.
105 Y. Yin, Z. Zhang, C. Xu, H. Wu, L. Shi, S. Wang, X. Xu, A. Yuan, S. Wang and H. Sun, *ACS Sustainable Chem. Eng.*, 2020, **8**, 823–830.
106 S. J. Geier, J. A. Mason, E. D. Bloch, W. L. Queen, M. R. Hudson, C. M. Brown and J. R. Long, *Chem. Sci.*, 2013, **4**, 2054–2061.
107 M. Mofarahi and S. M. Salehi, *Adsorption*, 2013, **19**, 101–110.
108 Y. Wang, S. Yuan, Z. Hu, T. Kundu, J. Zhang, S. B. Peh, Y. Cheng, J. Dong, D. Yuan, H.-C. Zhou and D. Zhao, *ACS Sustainable Chem. Eng.*, 2019, **7**, 7118–7126.
109 R.-B. Lin, H. Wu, L. Li, X.-L. Tang, Z. Li, J. Gao, H. Cui, W. Zhou and B. Chen, *J. Am. Chem. Soc.*, 2018, **140**, 12940–12946.
110 A. M. Plonka, X. Chen, H. Wang, R. Krishna, X. Dong, D. Banerjee, W. R. Woerner, Y. Han, J. Li and J. B. Parise, *Chem. Mater.*, 2016, **28**, 1636–1646.

111 J. Cai, J. Yu, H. Xu, Y. He, X. Duan, Y. Cui, C. Wu, B. Chen and G. Qian, *Cryst. Growth Des.*, 2013, **13**, 2094–2097.
112 O. T. Qazvini, R. Babarao, Z.-L. Shi, Y.-B. Zhang and S. G. Telfer, *J. Am. Chem. Soc.*, 2019, **141**, 5014–5020.
113 C. He, Y. Wang, Y. Chen, X. Wang, J. Yang, L. Li and J. Li, *Ind. Eng. Chem. Res.*, 2020, **59**, 6123–6129.
114 Y. Chen, Z. Qiao, H. Wu, D. Lv, R. Shi, Q. Xia, J. Zhou and Z. Li, *Chem. Eng. Sci.*, 2018, **175**, 110–117.
115 X. Wang, Y. Wu, X. Zhou, J. Xiao, Q. Xia, H. Wang and Z. Li, *Chem. Eng. Sci.*, 2016, **155**, 338–347.
116 J. Pires, M. L. Pinto and V. K. Saini, *ACS Appl. Mater. Interfaces*, 2014, **6**, 12093–12099.
117 F.-Z. Sun, S.-Q. Yang, R. Krishna, Y.-H. Zhang, Y.-P. Xia and T.-L. Hu, *ACS Appl. Mater. Interfaces*, 2020, **12**, 6105–6111.
118 H. Yang, Y. Wang, R. Krishna, X. Jia, Y. Wang, A. N. Hong, C. Dang, H. E. Castillo, X. Bu and P. Feng, *J. Am. Chem. Soc.*, 2020, **142**, 2222–2227.
119 U. Böhme, B. Barth, C. Paula, A. Kuhnt, W. Schwieger, A. Mundstock, J. Caro and M. Hartmann, *Langmuir*, 2013, **29**, 8592–8600.
120 M. Hartmann, U. Böhme, M. Hovestadt and C. Paula, *Langmuir*, 2015, **31**, 12382–12389.
121 H. Zeng, X.-J. Xie, M. Xie, Y.-L. Huang, D. Luo, T. Wang, Y. Zhao, W. Lu and D. Li, *J. Am. Chem. Soc.*, 2019, **141**, 20390–20396.
122 C. Gücüyener, J. van den Bergh, J. Gascon and F. Kapteijn, *J. Am. Chem. Soc.*, 2010, **132**, 17704–17706.
123 M. C. Das, H. Xu, Z. Wang, G. Srinivas, W. Zhou, Y.-F. Yue, V. N. Nesterov, G. Qian and B. Chen, *Chem. Commun.*, 2011, **47**, 11715–11717.
124 W. Liang, F. Xu, X. Zhou, J. Xiao, Q. Xia, Y. Li and Z. Li, *Chem. Eng. Sci.*, 2016, **148**, 275–281.
125 X.-Y. Li, Z.-J. Li, Y.-Z. Li, L. Hou, Z. Zhu and Y.-Y. Wang, *Inorg. Chem.*, 2018, **57**, 12417–12423.
126 Y. Chen, H. Wu, D. Lv, R. Shi, Y. Chen, Q. Xia and Z. Li, *Ind. Eng. Chem. Res.*, 2018, **57**, 4063–4069.
127 Z. Xu, X. Xiong, J. Xiong, R. Krishna, L. Li, Y. Fan, F. Luo and B. Chen, *Nat. Commun.*, 2020, **11**, 3163.
128 L. Yang, Y. Wang, Y. Chen, J. Yang, X. Wang, L. Li and J. Li, *Chem. Eng. J.*, 2020, **387**, 124137.
129 H. Wu, Y. Chen, D. Lv, R. Shi, Y. Chen, Z. Li and Q. Xia, *Sep. Purif. Technol.*, 2019, **212**, 51–56.
130 Y. He, Z. Zhang, S. Xiang, F. R. Fronczek, R. Krishna and B. Chen, *Chem. – Eur. J.*, 2012, **18**, 613–619.
131 Y. He, Z. Zhang, S. Xiang, F. R. Fronczek, R. Krishna and B. Chen, *Chem. Commun.*, 2012, **48**, 6493–6495.
132 L. Zhang, K. Jiang, L. Li, Y.-P. Xia, T.-L. Hu, Y. Yang, Y. Cui, B. Li, B. Chen and G. Qian, *Chem. Commun.*, 2018, **54**, 4846–4849.
133 L. Zhang, K. Jiang, J. Zhang, J. Pei, K. Shao, Y. Cui, Y. Yang, B. Li, B. Chen and G. Qian, *ACS Sustainable Chem. Eng.*, 2019, **7**, 1667–1672.
134 H. S. Scott, M. Shivanna, A. Bajpai, D. G. Madden, K.-J. Chen, T. Pham, K. A. Forrest, A. Hogan, B. Space, J. J. Perry Iv and M. J. Zaworotko, *ACS Appl. Mater. Interfaces*, 2017, **9**, 33395–33400.
135 J. W. Yoon, J. S. Lee, S. Lee, K. H. Cho, Y. K. Hwang, M. Daturi, C.-H. Jun, R. Krishna and J.-S. Chang, *Chem. – Eur. J.*, 2015, **21**, 18431–18438.
136 H.-M. Wen, H. Wang, B. Li, Y. Cui, H. Wang, G. Qian and B. Chen, *Inorg. Chem.*, 2016, **55**, 7214–7218.
137 D.-M. Chen, X.-H. Liu, J.-Y. Tian, J.-H. Zhang, C.-S. Liu and M. Du, *Inorg. Chem.*, 2017, **56**, 14767–14770.
138 F. Luo, C. Yan, L. Dang, R. Krishna, W. Zhou, H. Wu, X. Dong, Y. Han, T.-L. Hu, M. O'Keeffe, L. Wang, M. Luo, R.-B. Lin and B. Chen, *J. Am. Chem. Soc.*, 2016, **138**, 5678–5684.
139 H.-J. Lv, Y.-P. Li, Y.-Y. Xue, Y.-C. Jiang, S.-N. Li, M.-C. Hu and Q.-G. Zhai, *Inorg. Chem.*, 2020, **59**, 4825–4834.
140 Z. Yao, Z. Zhang, L. Liu, Z. Li, W. Zhou, Y. Zhao, Y. Han, B. Chen, R. Krishna and S. Xiang, *Chem. – Eur. J.*, 2016, **22**, 5676–5683.
141 X. Duan, Q. Zhang, J. Cai, Y. Yang, Y. Cui, Y. He, C. Wu, R. Krishna, B. Chen and G. Qian, *J. Mater. Chem. A*, 2014, **2**, 2628–2633.
142 Q. Dong, Y. Guo, H. Cao, S. Wang, R. Matsuda and J. Duan, *ACS Appl. Mater. Interfaces*, 2020, **12**, 3764–3772.
143 H. Cui, S. Chen, H. Arman, Y. Ye, A. Alsalme, R.-B. Lin and B. Chen, *Inorg. Chim. Acta*, 2019, **495**, 118938.
144 H. Yang, T. X. Trieu, X. Zhao, Y. Wang, Y. Wang, P. Feng and X. Bu, *Angew. Chem., Int. Ed.*, 2019, **58**, 11757–11762.
145 T. Xu, Z. Jiang, P. Liu, H. Chen, X. Lan, D. Chen, L. Li and Y. He, *ACS Appl. Nano Mater.*, 2020, **3**, 2911–2919.
146 J. Duan, W. Jin and R. Krishna, *Inorg. Chem.*, 2015, **54**, 4279–4284.
147 W. Fan, X. Wang, X. Liu, B. Xu, X. Zhang, W. Wang, X. Wang, Y. Wang, F. Dai, D. Yuan and D. Sun, *ACS Sustainable Chem. Eng.*, 2019, **7**, 2134–2140.
148 R. Liu, Q.-Y. Liu, R. Krishna, W. Wang, C.-T. He and Y.-L. Wang, *Inorg. Chem.*, 2019, **58**, 5089–5095.
149 H. Q. Wu, C. S. Yan, F. Luo and R. Krishna, *Inorg. Chem.*, 2018, **57**, 3679–3682.
150 Y.-P. Li, Y. Wang, Y.-Y. Xue, H.-P. Li, Q.-G. Zhai, S.-N. Li, Y.-C. Jiang, M.-C. Hu and X. Bu, *Angew. Chem., Int. Ed.*, 2019, **58**, 13590–13595.
151 Y. Ye, S. Chen, L. Chen, J. Huang, Z. Ma, Z. Li, Z. Yao, J. Zhang, Z. Zhang and S. Xiang, *ACS Appl. Mater. Interfaces*, 2018, **10**, 30912–30918.
152 Y. Ye, Z. Ma, R.-B. Lin, R. Krishna, W. Zhou, Q. Lin, Z. Zhang, S. Xiang and B. Chen, *J. Am. Chem. Soc.*, 2019, **141**, 4130–4136.
153 H. Li, H. Bonduris, X. Zhang, Y. Ye, A. Alsalme, R.-B. Lin, Z. Zhang, S. Xiang and B. Chen, *J. Solid State Chem.*, 2020, **284**, 121209.
154 L. Zhang, C. Zou, M. Zhao, K. Jiang, R. Lin, Y. He, C.-D. Wu, Y. Cui, B. Chen and G. Qian, *Cryst. Growth Des.*, 2016, **16**, 7194–7197.
155 P. Yan, J. Yang, X. Hao, Z. Chen, G. Shen, Y. Zhao, D. Ma and J. Zhu, *CrystEngComm*, 2020, **22**, 275–282.
156 H. Cui, Y. Ye, H. Arman, Z. Li, A. Alsalme, R.-B. Lin and B. Chen, *Cryst. Growth Des.*, 2019, **19**, 5829–5835.
157 L. Jiang, N. Wu, Q. Li, J. Li, D. Wu and Y. Li, *Inorg. Chem.*, 2019, **58**, 4080–4084.
158 G. Chang, B. Li, H. Wang, T. Hu, Z. Bao and B. Chen, *Chem. Commun.*, 2016, **52**, 3494–3496.
159 W. Fan, S. Yuan, W. Wang, L. Feng, X. Liu, X. Zhang, X. Wang, Z. Kang, F. Dai, D. Yuan, D. Sun and H.-C. Zhou, *J. Am. Chem. Soc.*, 2020, **142**, 8728–8737.
160 H. Zeng, M. Xie, Y.-L. Huang, Y. Zhao, X.-J. Xie, J.-P. Bai, M.-Y. Wan, R. Krishna, W. Lu and D. Li, *Angew. Chem., Int. Ed.*, 2019, **58**, 8515–8519.
161 X.-Y. Li, Y.-Z. Li, L.-N. Ma, L. Hou, C.-Z. He, Y.-Y. Wang and Z. Zhu, *J. Mater. Chem. A*, 2020, **8**, 5227–5233.
162 D.-Y. Ma, z li, J. Zhu, Y. Zhou, L. Chen, X. Mai, M. Liufu, Y. Wu and Y. Li, *J. Mater. Chem. A*, 2020, **8**, 11933–11937.
163 L. Li, J. Wang, Z. Zhang, Q. Yang, Y. Yang, B. Su, Z. Bao and Q. Ren, *ACS Appl. Mater. Interfaces*, 2019, **11**, 2543–2550.
164 M. L. Foo, R. Matsuda, Y. Hijikata, R. Krishna, H. Sato, S. Horike, A. Hori, J. Duan, Y. Sato, Y. Kubota, M. Takata and S. Kitagawa, *J. Am. Chem. Soc.*, 2016, **138**, 3022–3030.
165 R. Eguchi, S. Uchida and N. Mizuno, *Angew. Chem., Int. Ed.*, 2012, **51**, 1635–1639.
166 A. Cadiau, K. Adil, P. M. Bhatt, Y. Belmabkhout and M. Eddaoudi, *Science*, 2016, **353**, 137–140.
167 L. Yang, X. Cui, Z. Zhang, Q. Yang, Z. Bao, Q. Ren and H. Xing, *Angew. Chem., Int. Ed.*, 2018, **57**, 13145–13149.
168 H.-M. Wen, L. Li, R.-B. Lin, B. Li, B. Hu, W. Zhou, J. Hu and B. Chen, *J. Mater. Chem. A*, 2018, **6**, 6931–6937.
169 B. Chen, S. Xiang and G. Qian, *Acc. Chem. Res.*, 2010, **43**, 1115–1124.
170 Y. Wang and D. Zhao, *Cryst. Growth Des.*, 2017, **17**, 2291–2308.
171 S. Xiang, W. Zhou, J. M. Gallegos, Y. Liu and B. Chen, *J. Am. Chem. Soc.*, 2009, **131**, 12415–12419.
172 Q. Min Wang, D. Shen, M. Bülow, M. Ling Lau, S. Deng, F. R. Fitch, N. O. Lemcoff and J. Semanscin, *Microporous Mesoporous Mater.*, 2002, **55**, 217–230.
173 T. M. Nicholson and S. K. Bhatia, *J. Phys. Chem. B*, 2006, **110**, 24834–24836.
174 Z. Bao, S. Alnemrat, L. Yu, I. Vasiliev, Q. Ren, X. Lu and S. Deng, *Langmuir*, 2011, **27**, 13554–13562.
175 K. Lee, W. C. Isley, A. L. Dzubak, P. Verma, S. J. Stoneburner, L.-C. Lin, J. D. Howe, E. D. Bloch, D. A. Reed, M. R. Hudson, C. M. Brown, J. R. Long, J. B. Neaton, B. Smit, C. J. Cramer, D. G. Truhlar and L. Gagliardi, *J. Am. Chem. Soc.*, 2014, **136**, 698–704.
176 J. E. Bachman, D. A. Reed, M. T. Kapelewski, G. Chachra, D. Jonnavittula, G. Radaelli and J. R. Long, *Energy Environ. Sci.*, 2018, **11**, 2423–2431.
177 W. C. Zeise, *Ann. Phys.*, 1831, **97**, 497–541.
178 J. Chatt and L. A. Duncanson, *J. Chem. Soc. (Resumed)*, 1953, 2939–2947, DOI: 10.1039/JR9530002939.

179 S. Uchida, R. Kawamoto, H. Tagami, Y. Nakagawa and N. Mizuno, *J. Am. Chem. Soc.*, 2008, **130**, 12370–12376.
180 D. J. Safarik and R. B. Eldridge, *Ind. Eng. Chem. Res.*, 1998, **37**, 2571–2581.
181 S. Aguado, G. Bergeret, C. Daniel and D. Farrusseng, *J. Am. Chem. Soc.*, 2012, **134**, 14635–14637.
182 R. B. Eldridge, *Ind. Eng. Chem. Res.*, 1993, **32**, 2208–2212.
183 A. C. C. Campos, R. A. dos Reis, A. Ortiz, D. Gorri and I. Ortiz, *Ind. Eng. Chem. Res.*, 2018, **57**, 10071–10085.
184 Q.-Y. Yang, P. Lama, S. Sen, M. Lusi, K.-J. Chen, W.-Y. Gao, M. Shivanna, T. Pham, N. Hosono, S. Kusaka, J. J. Perry Iv, S. Ma, B. Space, L. J. Barbour, S. Kitagawa and M. J. Zaworotko, *Angew. Chem., Int. Ed.*, 2018, **57**, 5684–5689.
185 A. Schneemann, V. Bon, I. Schwedler, I. Senkovska, S. Kaskel and R. A. Fischer, *Chem. Soc. Rev.*, 2014, **43**, 6062–6096.
186 J. van den Bergh, C. Gücüyener, E. A. Pidko, E. J. M. Hensen, J. Gascon and F. Kapteijn, *Chem. – Eur. J.*, 2011, **17**, 8832–8840.
187 K. Kishida, Y. Watanabe, S. Horike, Y. Watanabe, Y. Okumura, Y. Hijikata, S. Sakaki and S. Kitagawa, *Eur. J. Inorg. Chem.*, 2014, 2747–2752.
188 S. Sen, N. Hosono, J.-J. Zheng, S. Kusaka, R. Matsuda, S. Sakaki and S. Kitagawa, *J. Am. Chem. Soc.*, 2017, **139**, 18313–18321.
189 S. Yang, J. Sun, A. J. Ramirez-Cuesta, S. K. Callear, W. I. F. David, D. P. Anderson, R. Newby, A. J. Blake, J. E. Parker, C. C. Tang and M. Schröder, *Nat. Chem.*, 2012, **4**, 887–894.
190 J. M. Michael and B. Smith, *March's Advanced Organic Chemistry*, Wiley, 6th edn, 2007, pp. 363–364.
191 W. S. W. Ho, G. Doyle, D. W. Savage and R. L. Pruett, *Ind. Eng. Chem. Res.*, 1988, **27**, 334–337.
192 K.-J. Chen, D. G. Madden, T. Pham, K. A. Forrest, A. Kumar, Q.-Y. Yang, W. Xue, B. Space, J. J. Perry Iv, J.-P. Zhang, X.-M. Chen and M. J. Zaworotko, *Angew. Chem., Int. Ed.*, 2016, **55**, 10268–10272.
193 S. K. Elsaidi, M. H. Mohamed, H. T. Schaef, A. Kumar, M. Lusi, T. Pham, K. A. Forrest, B. Space, W. Xu, G. J. Halder, J. Liu, M. J. Zaworotko and P. K. Thallapally, *Chem. Commun.*, 2015, **51**, 15530–15533.
194 A. Kumar, D. G. Madden, M. Lusi, K.-J. Chen, E. A. Daniels, T. Curtin, J. J. Perry Iv and M. J. Zaworotko, *Angew. Chem., Int. Ed.*, 2015, **54**, 14372–14377.
195 K.-J. Chen, R.-B. Lin, P.-Q. Liao, C.-T. He, J.-B. Lin, W. Xue, Y.-B. Zhang, J.-P. Zhang and X.-M. Chen, *Cryst. Growth Des.*, 2013, **13**, 2118–2123.
196 V. Bon, E. Brunner, A. Pöppl and S. Kaskel, *Adv. Funct. Mater.*, 2020, DOI: 10.1002/adfm.201907847.
197 N. Hosono, A. Terashima, S. Kusaka, R. Matsuda and S. Kitagawa, *Nat. Chem.*, 2019, **11**, 109–116.
198 S. Mukherjee, A. V. Desai and S. K. Ghosh, *Coord. Chem. Rev.*, 2018, **367**, 82–126.
199 X. Han, S. Yang and M. Schröder, *Nat. Rev. Chem.*, 2019, **3**, 108–118.